Recking, A. (2013), An analysis of nonlinearity effects on bed load transport prediction,
J. Geophys. Res. Earth Surf., 118, doi:10.1002/jgrf.20090.

An analysis of nonlinearity effects on bedload transport prediction

A. Recking, IRSTEA, UR ETGR, 2 Rue de la Papeterie, BP76, 38402 Saint Martin d'Hères, France. E-mail: alain.recking@irstea.fr

Recking, A. (2013), An analysis of nonlinearity effects on bed load transport prediction,
J. Geophys. Res. Earth Surf., 118, doi:10.1002/jgrf.20090.

ABSTRACT

Because bedload equations are nonlinear and because parameters describing the flow and the bed can have large variance, different results are expected when integrating bedload over a cross section with respect to spatially variable local data (2D), or when computing bedload from cross-section-averaged data, which reduces the problem to uniform conditions (1D). Evidence of these effects is shown by comparing 1D (flume-derived) equations with 2D field measurements, and by comparing a 2D (field-derived) equation with 1D flume measurements, leading to the conclusion that different equations should be used depending on whether local or averaged data are used. However, whereas nonlinearity effects are considerable for low-transport stages, they tend to disappear for higher flow conditions.

Probability distribution functions describing the variance in flow and bed grain size distribution (GSD) are proposed and the width-integrated bedload data (implicitly containing the natural variance in bed and flow parameters) are used to calibrate these functions. The method consists of using a Monte Carlo approach to match the measured 2D bedload transport rates with 1D computations, artificially reproducing the natural variance associated with the mean input parameters. The Wilcock and Crowe equation was used for the 1D computation because it was considered representative of 1D transport.

The results suggest that nonlinearity effects are mostly sensitive to the variance in shear stress, modeled here with a gamma function, whose shape coefficient α was shown to increase linearly with the transport stage. This variance in shear stress suggests that even for very low flow conditions, shear stress can locally exceed the critical shear stress for the bed armor, generating local armor break-up. This could explain why the bedload GSD is usually very similar to subsurface GSD, even in the presence of complete armor.

INTRODUCTION

Bedload transport prediction is important for many applications, including river engineering, hazard prediction, and environmental monitoring and management. Sophisticated equations have been proposed in recent decades [*Parker*, 1990; *Wilcock and Crowe*, 2003], and when the quality of the required input data is good and the flow hydraulics are calculated in sufficient detail to take into account shear stress variations, they have been shown to adequately predict transport rates, changes in bed topography, and downstream fining [*Ferguson and Church*, 2009]. However, the requisite data (detailed grain size distribution [GSD], topography, discharge or depth) are not always available, and in many practical situations bedload must be computed with limited information and width-averaged river characteristics: The GSD is reduced to a few surface diameters (D_{50}, D_{84}), often estimated by surface counting [*Wolman*, 1954], the bed topography is assumed to be trapezoidal or rectangular and reduced to a mean width W and slope S, and the flow is considered uniform at the reach scale (a single water depth d for a given discharge and the energy slope equal to the bed slope).

Despite reflecting the reality of many practical situations, the proposed approach of computing bedload with simple models and width-averaged data has been widely criticized for two main reasons: First, equations using limited input data are assumed to be incapable of reproducing the full complexity of transport [*Habersack and Laronne*, 2002], and second, since bedload equations are nonlinear with exponents that may exceed values of 10, width-averaged bedload calculation has been suspected of under-estimating the true bedload flux if there is any local and/or spatial variation in either the bed material size distribution or in the flow hydraulics [*Gomez and Church*, 1989; *Paola and Seal*, 1995; *Ferguson*, 2003; *Bertoldi, et al.*, 2009; *Francalanci, et al.*, 2012].

Ferguson [2003] demonstrated nonlinearity effects with an analytical model based on the Meyer–Peter and Mueller formulation (derived for local transport in a flume). Using a probability function describing the shear stress variation around its mean value, he showed that additional flux locally induced by high shear stress outweighs the lower flux induced by low shear stress and that, consequently, the total flux (the sum of all local fluxes) should be higher than the flux computed with the averaged shear stress. These effects are illustrated in Figure 1, where τ^* is the Shields number, which for diameter D is:

$$\tau^* = \frac{RS}{(s-1)D} \quad (1)$$

where R is the hydraulic radius, S is the slope, and $s=\rho_s/\rho$ is the ratio between the sediment and the water density. Figure 1a illustrates a river section, the averaged Shields stress $<\tau^*>$ and computed bedload transport $q_s(<\tau^*>)$, and its decomposition in local values τ_i^* and $q_s(\tau_i^*)$; whereas the local shear stress τ_i^* is twice the average value $<\tau^*>$ in the figure, the corresponding computed bedload transport is plotted such that $q_s(\tau_i^*) >> 2q_s(<\tau^*>)$. These effects occur because bedload has been shown to be a power function of the shear stress and the value of the exponent is greater than 1. Considering $q_s \propto \tau^{*p}$, Figure 1b shows that the higher the value of the exponent p, the greater these effects (with a threshold equation of the form $q_s \propto (\tau^* - \tau_c^*)^p$ these effects would be maximum near the critical Shields stress τ_c^*).

In contrast to the above expectation, most studies comparing bedload equations to measured bedload transport rates report large over-estimates instead of under-estimates when equations are used with width-averaged data, especially for gravel bed rivers [*Rickenmann*, 2001; *Barry, et al.*, 2004; *Bathurst*, 2007; *Recking, et al.*, 2012]. In addition, because equations derived on the basis of field data are supposed to have a built-in allowance for the effects of spatial variability, they should considerably improve the computation of bedload transport when compared with standard 1D equations; however, many equations based on

field data are also site specific, and *Barry et al.* [2004; 2007] did not draw any conclusions about the superiority of one category of equation when compared with field data.

Consequently, the questions this paper aims to answer are: How do the nonlinear effects influence predicted transport rates? Can a single equation, used with either the exact local shear stress or with width-averaged river characteristics, reproduce local transport and width-averaged transport, respectively, or should we consider two distinct families of equations, depending on whether bedload must be computed with local shear stress (as in numerical models) or with width-averaged data? Can we relate nonlinearity effects to the natural variance in flow and bed parameters?

First, flume and field data are presented. Secondly, they are used with several bedload transport equations (1D capacity equation, 1D surface-based equation, and 2D field-derived equation) to look for evidence of nonlinearity effects. Thirdly, the variance associated with each flow and bed parameter is described, and a Monte Carlo approach is used for statistically investigating (calibrating) the shape parameter of each probability distribution function. Finally, the results are used to discuss the use of equations in field applications.

DATA SET PRESENTATION

In this part, the data set used in the analyses is presented; field data are considered 2D data because they are width-integrated, and they are distinguished from flume data that are considered 1D (near-uniform) and therefore an analogue for local transport in natural rivers. Note that the term 1D should rigorously correspond to strictly uniform flows (constant depth and bed roughness); however, such flows are almost never fully observed even in the flume, where small bedforms can exist and sediment patches can develop [*Meyer-Peter and Mueller*, 1948; *Dietrich, et al.*, 1989]. Consequently 1D flow is used here to designate quasi-uniform flows when compared with 2D flows in the field.

All parameters considered width-averaged are noted between the symbols < >; other standard notations correspond to local values. The flow conditions were discriminated with the transport stage defined by the τ^*/τ_c^* ratio [*Church and Zimmerman*, 2007], where τ_c^* is the critical Shields stress estimated with the following formula fitted to a compilation of field data from the literature [*Recking*, 2009]:

$$\tau_{ci}^* = (1.32S + 0.037)\left(\frac{Di}{D_{50}}\right)^{-0.93} \quad (2)$$

Large uncertainties exist on τ_c^* [*Buffington and Montgomery*, 1997] and a constant and arbitrary value τ_c^*=0.03 [*Parker, et al.*, 2003] or 0.047 [*Meyer-Peter and Mueller*, 1948] could have been used, but using a dependency with slope is more likely to represent reality [*Mueller, et al.*, 2005; *Lamb, et al.*, 2008; *Recking*, 2009; *Ferguson*, 2012]. The transport stage can be defined for different diameters D_i. D_{50} was used because this diameter is often considered representative. However, because the exponent in Eq. 2 is near 1, the results would have been slightly changed with other diameters such as D_{84} (used for plotting the data in Recking et al. 2012). Nonetheless, this is not important because this choice impacts only the distribution of the results on the figures (the x-axes) and not the results themselves (all equations being used exactly as recommended by their authors).

1D data

Investigating local transport assumes knowledge of the local values. Whereas a few field data sets measure local transport and the associated flow velocity, the bed surface GSD is always highly uncertain and always averaged at the reach scale. Such local data sets would be very difficult to construct because measuring the local bed GSD associated with transport is almost impossible during flooding. A practical way to obtain such information is flume experiments, where the flow can be stopped and the bed can be sampled after each bedload measurement, as done by *Wilcock et al.* [2001]. They produced bedload data in a 0.6-m-wide and an 8-m-long tilting flume, with recirculation of poorly sorted sediment mixtures and flow

conditions allowing partial transport. Five runs were produced with different sand contents and the data are summarized in Table 1 and are available in *Wilcock et al.* [2001]. These data cover a large slope range (0.06%–2%) and are (to the best of the author's knowledge) the only published flume data that fully document partial transport [*Wilcock and McArdell*, 1993]. These flows are not strictly speaking 1D, as uniformity implies a perfectly constant water depth and bed roughness. However, as mentioned by the authors, "*the sediment bed was essentially planar,*" which allows for the hypothesis of near-uniform flows when compared with flows in a natural river reach.

2D data

An existing field data set comprising 6,319 values (available in *Recking*, [2010]) was expanded with new data from the literature comprising 2,614 measurements collected on 24 river reaches. The main characteristics of this new data set are given in Appendix A and the data (including bed surface GSD) are available on-line as supplementary material. The complete data set comprises 8,940 values collected at 109 river sites and is summarized in Table 2. Most sampling results (when specified) provided width-averaged data for the bed GSD, the flow characteristics (discharge, velocity), and the bedload transport. The following figures provide general descriptions of the data set and were used in the subsequent calculations of 2D bedload transport.

Figure 2 presents the cumulative distribution of diameter $<D_{84}>$, slope $<S>$, and width $<W>$ for the 109 reaches composing the data set. Only 5% are sand bed rivers and 10% have a D_{84} smaller than 1 cm (not many published bedload data collected on sand bed rivers were found in the literature); 70% are gravel bed rivers and 20% are cobble and boulder bed rivers. Slopes span a broad range of values from 0.01 to 8%. Most widths are in the range 0–15 m, but reaches as large as 500 m were also considered. The different ranges obtained for $<D_{84}>$, slope $<S>$, and width $<W>$ are consistent, with width and grain size evolving with slope, from

large lowland sandy rivers to steep narrow boulder streams [*Montgomery and Buffington*, 1997; *Church and Zimmerman*, 2007]. Figure 3 plots slope $< S >$ as a function of $<D_{84}>$ for the data set considered; the trend roughly follows a power function.

A selection of 121 GSDs are plotted in Figure 4. Figure 4a plots a selection of 78 GSDs collected in gravel bed rivers (from the Idaho data set; *King et al.* [2004]) and the corresponding averaged GSD. It shows a similar shape between all curves. Figure 4b plots 42 additional GSDs, including sand bed rivers. Figure 4 indicates that the sand fraction at the bed surface $\langle F_s \rangle$ can vary greatly, and these data suggest $0 < \langle F_s \rangle < 0.2$ for most gravel bed rivers. This is confirmed in Figure 5, where $\langle F_s \rangle$ is plotted as a function of $\langle D_{84} \rangle$: It is close to 1 for sand bed rivers and rapidly decreases to approximately 0.1–0.15 for gravel bed and cobble bed rivers.

Figure 6 (that also includes additional data from *Pitlick et al*., [2008]) indicates that the $\langle D_{84} \rangle / \langle D_{50} \rangle$ ratio is approximately equal to 2, which was also found to be representative of gravel bed rivers by *Rickenmann and Recking* [2011] with another data set. However, the ratio can also differ significantly from 2, and $\langle D_{84} \rangle / \langle D_{50} \rangle = 2$ is associated with a variance following approximately a log-normal distribution with a standard deviation σ_{DR} =0.3 ($1.1 < D_{84}/D_{50} < 3.3$).

Figure 7 presents relations between the transport stage and the bed surface $<D_{84}>$ and the slope. It indicates a decrease of $<\tau^*>/<\tau_c^*>$ with $<D_{84}>$ following roughly a power law (R^2=0.45); a similar relation does not seem to exist with the slope. Low $<\tau^*>/<\tau_c^*>$ values for high $<D_{84}>$ values is not surprising, as the Shields number $<\tau^*>$ is known to barely exceed 120% of the critical value $<\tau_c^*>$ in gravel bed rivers [*Parker*, 1978; *Andrews*, 1983; *Ryan, et al.*, 2002; *Mueller, et al.*, 2005; *Parker, et al.*, 2007]. In fact, only for sand and fine gravels can the transport stage be very high [*Buffington*, 2012].

Figure 8a plots the unit transport rates $<q_s>$ (g/s/m) and Figure 8b plots the averaged dimensionless transport $<\Phi>$, with Φ defined by [*Einstein*, 1950]:

$$\Phi = \frac{q_s}{\rho_s \sqrt{g(s-1)D_{50}^3}} \quad (3)$$

where ρ_s is the sediment density. Transport rates cover a wide range; it is interesting to note that the threshold value $<\tau^*>/<\tau_c^*>=1$ (computed for D_{50}) corresponds to somewhat considerable transport and $<\tau^*>/<\tau_c^*>=2$ approximately delimits two groups with a change in trend, a result which is consistent with previous analyses [*Parker, et al.*, 1982; *Buffington*, 2000].

To complete this description of the field data, the bed morphology should be presented. Unfortunately, except for a few cases [*Hassan and Church*, 2001; *Church and Hassan*, 2002], an exact description of the reach used for measurements was usually not included in the publications. Mostly only general descriptions of river morphology were provided, but available information suggests that straight reaches were frequently chosen for bedload measurements. Nevertheless, the surrounding reach morphology of some sites may exhibit substantial topographic variation (e.g., pool-riffle or step-pool channels).

LOOKING FOR EVIDENCE OF NONLINEARITY EFFECTS

In this part, the flume and the field data are used with bedload equations to look for evidence of nonlinearity effects. Bedload equations are used exactly as recommended by their authors.

From the flume to the field

This part aims to analyze whether averaging the data produces under-prediction when 1D equations are used in the field.

Sixteen flume-derived 1D bedload transport equations were compared with a large field data set in *Recking et al.* [2012]. The conclusion of this study was that for the lowest transport stages (corresponding to partial transport, with $\tau^*/\tau_c^* < 1$ for the coarser fractions),

these threshold equations predicted zero transport whereas the measured transport was non-zero. When the non-zero transport computations were considered, the results showed over-estimation, for all equations, often by several orders of magnitude, which is not in accordance with the expected under-estimation induced by nonlinearity. This resulted in a generally poor performance of most of the equations tested, except for high flow conditions (when $\tau^*/\tau_c^* > 2$, which corresponds to sand and fine gravels in Figure 7a). One reason potentially responsible for over-prediction is that these equations do not account for the changing critical shear stress with slope.

To overcome this threshold problem (zero prediction and slope effects), a 1D bedload equation expressed as a function of τ^*/τ_c^* was fitted in *Recking* [2010] on a large flume data set obtained with near-uniform sediments (compilation comprising most of the data that have served to build the equations reported in the literature, available as supplementary material in *Recking*, [2010]). This equation accounts for variation of the critical Shields stress with slope and is presented in Appendix B1. When this 1D equation (used with the median diameter) is compared with the 1D flume data from *Wilcock et al.* [2001], the results plotted in Figure 9 can be deemed satisfying, considering that there was no calibration; most particularly, the trend is very good and there is no clear evidence for over- or under-prediction.

On the other hand, when this equation is compared with the field data, the results plotted in Figure 10 clearly confirm under-prediction when the transport stage is $\tau^*/\tau_c^* < 0.7$, as expected by nonlinearity effects. However, like the other equations tested in *Recking et al*. [2012], this equation over-estimates transport rates for higher flow conditions and gives acceptable results only when $\tau^*/\tau_c^* > 2$ approximately. The possible reason for over-estimation in the range $0.7 < \tau^*/\tau_c^* < 2$ is that all these equations were derived to match as well as possible the transport capacity of nearly uniform fine materials in flume experiments (see *Recking et al.* 2008 for a review of these data). In these conditions, each increment in

shear stress was systematically balanced by an increment in transport. In gravel and cobble bed rivers, sediments are not always available for transport because of supply limitations and hiding effects, and small increments in shear stress may not be compensated by an immediate increment in bedload, which can explain over-estimation [*Bathurst*, 2007; *Recking*, 2012]. The results are improved in the range $1 < \tau^*/\tau_c^* < 2$ when the Meyer–Peter and Mueller [1948] shear stress correction is used; however, it also considerably increases under-prediction in the $\tau^*/\tau_c^* < 1$ range.

To overcome the above-mentioned problem, fractional equations were developed for computing the transport of what is actually present on the bed surface [*Parker and Klingeman*, 1982; *Parker*, 1990; *Wilcock and Crowe*, 2003]. Among these equations, the Wilcock and Crowe [2003] equation is considered a truly surface-based relation [*Parker*, 2009] because it was derived from the flume experiments of *Wilcock et al.* [2001], with the exact surface GSD being measured immediately after each flow event. This equation (presented in Appendix B2) was used as suggested by the authors, with the GSDs sampled at 1-ψ intervals, and by computing the grain shear stress with $\tau = 17(SD_{65})^{1/4}U^{3/2}$ [*Wilcock, et al.*, 2009]. A comparison with the field data set (restricted to 82 reaches and 6,239 values because the full GSD was not available for all data) showed no significant over-prediction and a tendency for under-prediction at low shear stresses, in agreement with expected nonlinearity effects (Figure 11). Similar results were obtained by *Gaeuman et al.* [2009] who compared the Wilcok and Crowe equation to bedload measurements of the Trinity river.

To conclude, the above analysis suggests that the variance in flow and bed parameters produces under-prediction at low transport stages when 1D equations are used in the field.

From the field to the flume

A second way to verify the effects of nonlinearity is to use a 2D field-derived equation for computing local transport. By fitting the width-integrated transport measurements, these

equations have a built-in allowance for the effects of spatial variability, which should improve the computation of field bedload transport with width-averaged input data, when compared with standard 1D equations. On the other hand, if they implicitly compensate for spatial variability, these equations should logically over-predict transport when compared with 1D measurements because of nonlinearity effects. This is what was tested here by comparison with the flume data from *Wilcock et al.* [2001] (assuming that these data are representative of 1D transport in the field).

Several 2D field-derived equations have been proposed in the literature [*Parker, et al.*, 1982; *Barry, et al.*, 2008; *Recking*, 2010]. Here, an equation (presented in Appendix B3) proposed in a previous paper by the author [*Recking*, 2013] was used because it requires only a few parameters and permits a direct comparison with flume data. This equation was compared with the field data set (restricted to 5,735 values not used in its construction, collected at 73 sites, for blind testing), and the results plotted in Figure 12 indicates only a slight under-prediction at very low Shields stress ratios. The comparison with a selection of river reaches did not indicate any particular dependency on the bed morphology (Figure 13). On the other hand, the comparison with 1D flume data confirmed over-prediction for the low transport stages, as expected by nonlinearity effects (Figure 14).

To conclude this part, only low transport stages are affected by nonlinearity effects. Assuming that the flume data are representative of local flows, this analysis suggests that the variance in flow and bed parameters produces under-prediction when 1D equations are used in the field. Field-derived equations compensate for these effects, but by contrast they over-predict bedload transport when they are used for computing local transport with local flow values (e.g., in a numerical model). The following section aims to fill the gap between 1D and 2D transport by investigating the variance associated with each parameter.

INVESTIGATING THE MISSING DIMENSION

The difference between 1D bedload computation and 2D bedload measurements results from variance in shear stress and bed properties. Each bedload value of the data set is by construction the average of several bedload values measured locally and produced by the variance in flow and bed GSD (as illustrated in Figure 1a); consequently, bedload data implicitly include the variance in flow and bed parameters, which evolve in both space and time. On the other hand, this variance is absent from the associated flow and bed data (discharge measured not simultaneously and often at a gauging station, in another location, and with a single mean GSD). This variance, which is present in bedload data and absent in the flow and bed data used in the equations, is what *Ferguson* [2003] called the "missing dimension."

The only way to make the use of a 1D equation consistent for comparison with measured 2D field data would be to "artificially" reproduce the natural flow and bed variability. This is done in this part of the paper, using the averaged input data in the 1D Wilcock and Crowe equation, with their variance described by probability distribution through a Monte Carlo approach.

Probability distribution functions describing the variance in flow and bed parameters

The depth $\langle d \rangle$ can vary considerably in an irregular cross section, ranging from near zero close to the banks to a maximum at the thalweg, and is linearly related to shear stress for a given slope $\langle \tau \rangle \propto \langle S \rangle \langle d \rangle$. The variance associated with longitudinal slope across a given cross section is difficult to evaluate; however, as pointed out by *Ferguson* [2003], available field studies have actually shown a positive correlation between d and τ (local deviations from $\tau \propto d$ tending to cancel each other out), leading to a similar frequency distribution for d and τ. This is why in the following the variance was considered directly for the shear stress $\langle \tau \rangle$ instead of separate variance for $\langle d \rangle$ and $\langle S \rangle$. This variance was described with an

asymmetric gamma probability function, as already proposed in other works [*Paola*, 1996; *Nicholas*, 2000; *Bertoldi, et al.*, 2009]:

$$p(\tau) = \frac{\alpha^{\alpha}\hat{\tau}^{\alpha-1}e^{-\alpha\hat{\tau}}}{\langle\tau\rangle\Gamma(\alpha)} \quad (4)$$

where $\hat{\tau} = \tau/\langle\tau\rangle$, $\langle\tau\rangle$ is the width-averaged bed shear stress, and α is a parameter describing the width of the distribution. The lower its value, the larger the variance in τ. A value α=1 was found to be a limiting value for highly irregular cross sections [*Paola*, 1996; *Nicholas*, 2000], for instance, in braided streams. It also predicts a shear stress in the range $0 < \tau/\langle\tau\rangle < 5$ (Figure 15), which is approximately what *Ferguson* [2003] obtained with his probability function when the shear stress is below its mean value of over 80% of the cross section. Values greater than 5 would be representative for single-thread irregular channels, and α tends toward infinity for a rectangular cross section.

Fractional equations require a complete definition of the GSD. Instead of discussing the variance associated with each size class, GSD was reduced to three parameters: the sand fraction on the bed surface *Fs*, the median diameter D_{50}, and the D_{84}/D_{50} ratio. This model, presented in Table 3, was obtained by considering the proportionality ratios between each size class measured in the compilation of 78 GSDs, plotted in Figure 4a. Figure 16a shows three examples of measured GSDs and their approximation with the model, and Figure 16b and c indicates that the difference between the measured and computed percentage for each fraction of the whole data set is very weak. There is no intention here to reduce all natural GSDs to these three parameters, but it allows very realistic GSDs to be built.

Only a few studies have investigated the variability of GSDs in a given reach [*Church and Kellerhalls*, 1978; *Crowder and Diplas*, 1997], and defining the variance for *Fs*, D_{50}, and D_{84}/D_{50} for the purpose of this study is not trivial. Considering the central limit theorem, the distribution of the means of a series of samples should be normally distributed regardless of the underlying distribution of the sample; therefore it is hypothesized that for a given mean

value $\langle D_{50} \rangle$, diameters D_{50} vary randomly following a normal distribution (Figure 17). Several values were considered for standard deviation σ_D. The value $\langle D_{84} \rangle / \langle D_{50} \rangle = 2$ and the associated normal distribution ($\sigma_{DR} = 0.3$) observed between sites (Figure 6) was hypothesized as always valid, including for different locations in a given site. Fs=0.1 was considered on average for gravel bed rivers (Figure 5); however, sand can be either uniformly distributed over the surface or concentrated in local patches [*Buffington and Montgomery*, 1999a; *Dietrich, et al.*, 2006], which can be described with an asymmetric beta function $B(x_1,x_2)$, with an average set to $x_1/x_2 = 0.1$ (where x_1 and x_2 are the shape parameters of the function). Figure 18 plots $B(x_1, x_2)$ for different values of x_1 and x_2. Low coefficients ($x_1 = 0.001$; $x_2 = 0.01$) simulate near-zero sand everywhere and high local sand concentration (patches); on the other hand, high coefficients (x_1=100 and x_2=1000) simulate a more uniform distribution of the sand fraction over the surface.

Limited evidence of a clear correlation between grain size and depth led Ferguson [2003] to consider two limiting scenarios: purely random patchiness, and perfect fining upward as in classic models of meander point bars. Here, only the case of near-straight reaches was considered, with no or little correlation between grain size and depth. Flows over typical morphological units such as riffle, pools, and bars are considered in the discussion.

A Monte Carlo approach for calibrating the probability functions

In this section the width-integrated bedload data (implicitly containing the natural variance in bed and flow parameters) were used to calibrate the probability functions describing the variance in flow and bed parameters. This approach is in a sense similar to that of *Chiari and Rickenmann* [2010], who used bedload measurements for back-calculating the macro roughness of several alpine rivers; however, whereas they used a numerical model, a Monte Carlo approach was used here.

348 For a given set of width-averaged input data (say, $\langle F_s \rangle, \langle D \rangle, \langle \tau \rangle$), the Monte Carlo
349 approach consists in performing a large number of random draws from the probability
350 distribution of each input parameter to construct numerous sets of local values (*Fs*, *D*, τ)
351 about the means. In the second step, each set of local values is used in the 1D bedload
352 equation to compute the associated local bedload transport q_s. Assuming the probability
353 distribution functions are correct, averaging these local bedload values $\frac{1}{N}\sum_N q_s$ should
354 retrieve (in a statistical sense) the measured (and width-averaged) bedload transport $q_{s\,meas}$.
355 For each flow range (considered through the ratio $\langle \tau^* \rangle / \langle \tau_c^* \rangle$) and given values of $\langle S \rangle$,
356 $\langle F_s \rangle$, $\langle D_{50} \rangle$, and $\langle D_{84} \rangle / \langle D_{50} \rangle$, the different steps are:
357 (1) computation of $\langle \tau^* \rangle$ for each transport stage $\langle \tau^* \rangle / \langle \tau_c^* \rangle$ (considered for values 0.3, 0.5,
358 0.7, 1, 1.3, 1.5, 2, 5, and >5) knowing $\langle \tau_c^* \rangle$ (given by Eq. 2), from which we deduce
359 $\langle R/D_{84} \rangle = 1.65 < \tau^* > / < S >$ (Eq. 1);
360 (2) calculation of the flow velocity $\langle U \rangle$ for $\langle R/D_{84} \rangle$ with the *Ferguson* [2007] flow
361 resistance equation (this equation was chosen because it has been shown to give satisfying
362 values when compared with a large data set in *Rickenmann and Recking*, [2011]);
363 (3) calculation of the appropriate mean grain shear stress $\langle \tau \rangle = 17\left(\langle S \rangle \langle D_{65} \rangle\right)^{1/4} \langle U \rangle^{3/2}$
364 [*Wilcock, et al.*, 2009]; $<D_{65}>$ is given in millimeters and deduced from the model of Table 3;
365 (4) construction of several sets of local values for τ and *GSD* (with the model of Table 3) by
366 random draws in the probability distributions of $\langle \tau \rangle$ and $\langle F_s \rangle, \langle D_{50} \rangle, \langle D_{84}/D_{50} \rangle$;
367 computation of the associated bedload $q_s(\tau, GSD)$ with the Wilcock and Crowe equation.
368 Large data sets (*N*=5,000) were constructed to ensure a stable solution for the computed
369 bedload probability distribution;

(5) calculation of the average value $\langle q_s(\tau, GSD)\rangle = \frac{1}{N}\sum_N q_s(\tau, GDS)$;

(6) comparison of $\langle q_s(\tau, GSD)\rangle$ with $q_{s\,meas}$.

Results of simulations

The simulations were tested with different values for α (for τ), σ_D (for D_{50}), and x_1 (with $x_2 = 10x_1$ for $<F_s> = 0.1$). Figure 19 compares the $q_s(\langle\tau^*\rangle)/q_{s\,meas}$ ratios (where $q_{s\,meas}$ is the measured bedload transport and $q_s(\langle\tau^*\rangle)$ is bedload computed with the Wilcock and Crowe equation used with average input data, as shown in the right panel of Figure 11) with $q_s(\langle\tau^*\rangle)/<q_s(\tau^*)>$, where $<q_s(\tau^*)>$ is the average bedload deduced from the Monte Carlo computation. Adequate probability distributions should make it possible to fit $<q_s(\tau^*)>$ with $q_{s\,meas}$ (in a statistical sense).

No stable solution could be obtained with $\sigma_D > 0.3$ (leading to near-zero D_{50}), and simulations were considered with $0.1 < \sigma_D < 0.3$. This range is consistent with *Segura et al.* [2010], who measured σ_D in the range 0.1–0.36 on the basis of multi-pebble counts [*Wolman*, 1954] involving 2,500–4,700 particles on three reaches of the Williams Fork River (Colorado, USA). It is also consistent with measurements made on a large gravel bar on the Gunnison River [*Barkett*, 1998], a tributary to the Colorado River, consisting of 28 separate Wolman counts of 100 particles each (total of 2,800 particles), and for which σ_D was 0.28 (*John Pitlick*, personal communication).

Figure 19a shows that it was not possible to match the measurements for all flow conditions when setting a constant α-value ($\alpha = 1$ actually seems to work fairly well as a lower limit to the data). As a consequence, α was empirically varied with the transport stage $\langle\tau^*\rangle/\langle\tau_c^*\rangle$ in Figure 19 b and c. All combinations (α, σ_D, x_1) were tested with $\langle\tau^*\rangle/\langle\tau_c^*\rangle$ within the range [0.3–100], for constant slopes $<S>$ and $<D_{50}>$ (Figure 19b) and also with the

transport stage $\langle \tau^* \rangle / \langle \tau_c^* \rangle$ linked to the slope and GSD (Figure 19c) through relations plotted in Figure 3 and Figure 7a. Whatever the hypothesis, the best fit between computed (with the Monte Carlo approach) and measured bedload was obtained by varying α linearly with a function given in the form (Figure 19b and c):

$$\alpha = \xi \frac{\langle \tau^* \rangle}{\langle \tau_c^* \rangle} \tag{5}$$

The value of ξ in Equation 5 is slightly sensitive to the variance in GSD. A value of 5 best fits the measured bedload transport with σ_D =0.1 (Figure 19c), and a value of approximately 8–10 (not shown in the figure) would be more appropriate for a higher variance in D_{50} (σ_D =0.25). Results plotted in Figure 19c indicate a weak dependency on whether sand is considered uniformly displayed over the surface (x_1=100, x_2=1000) or is concentrated into patches (x_1=0.001, x_2=0.01).

The conclusion from these simulations is that predictions are weakly sensitive to the variance in GSD (Figure 19 b and c) but very sensitive to the variance in shear stress (Figure 19a). Such an increase in the parameter α with flow strength was an expected result [*Nicholas*, 2000], and values within the range $2 < \alpha < 10$ are consistent with results for single-thread channels found by *Tunnicliffe et al.*[2012].

DISCUSSION

Consequences for field application

The above results suggest that all models are not adapted to all situations. 1D equations used with width-average input data are likely to under-estimate width average bedload transport. The Monte Carlo approach (used with appropriate probability distributions) can be used for compensating the "missing dimension." It is illustrated hereafter with the example of the Lochsa River (using hydraulics and bedload data presented in *King et al.* [2004]).

For the given bed characteristics (F_s=0.03, D_{50}=0.126 m, D_{84}=0.28m, S=0.0023), the procedure has consisted in defining, for each of the 71 runs characterized by a measured velocity U and depth d, the transport stage $<\tau>/<\tau_c>$, the GSD, the probability distribution for all parameters (no calibration was used here, and α=5, σ_D=0.1, σ_{DR}=0.3, x_1=100 and x_2=1,000 following the above results), and in building bedload data with the Wilcock and Crowe equation (3,000 values were computed for each run), which were averaged and compared with the measured bedload.

The results presented in Figure 20 indicate that taking into account the variance in bed and flow parameters can greatly improve prediction when compared with a direct computation of the width-averaged data. The inconvenience of this approach is that thousands of calculations are needed for each width-averaged input data considered.

Local vs. averaged shear stress

Testing the equations (Figure 11) and the Monte Carlo results (Figure 19) showed that the under-prediction is greater for low transport stages and decreases with increasing shear stress, as *Ferguson* [2003] also concluded. This can be explained by a reduced variance in the shear stress when the flow increases, because depth variations with the local bed topography may become relatively negligible with regard to the mean flow depth (this is particularly true for moveable beds becoming flatter with increasing transport stage).

Equations 4 and 5 were used to compute the distribution of the local transport stage $\tau/<\tau_c>$, for different values of the mean transport stage $<\tau>/<\tau_c>$. The results, plotted in Figure 21, indicate that for $<\tau>/<\tau_c>$ ratios as low as 0.3, the shear stress may locally be higher than the critical shear stress for mobility of the bed surface (τ/τ_c>1). This means that local armor break-up can always exist to some degree, exposing the subsurface material to the flow. This finding is consistent with the observation that even in the presence of a coarse armor, with a zero sand fraction at the bed surface (F_s = 0), the bedload GSD is always much

finer than the surface GSD and equivalent to the subsurface GSD. This was, for instance, the case for several of the Idaho streams [*King, et al.*, 2004], for which bedload was measured for very low transport stages. However, the bedload material may also include upstream sediment supply that is not accounted for in the current analysis. Consequently, the sand fraction measured at the bed surface at rest could be an incorrect indicator of sediment availability for bedload computation.

Several questions to be investigated further

The first question is how much are the above results dependent on the Wilcock and Crowe equation, used here as representative of 1D transport? To answer this question, another 1D equation was considered. In work not shown here, an attempt was made to adapt the 2D Recking [2013] equation (Appendix B3) to 1D transport by introducing a correction coefficient $\zeta < 1$ such that:

$$\Phi_{1D} = \zeta(\tau^*, F_s)\Phi_{2D} \quad (6)$$

According to Figure 14, the function $\zeta(\tau^*, F_s)$ must converge to 1 when the sand fraction F_s converges to 1 or when the transport value is high (when all grain classes are moving, which can be expressed, for instance, with reference to the threshold conditions τ_c^* for the coarser fraction considered through diameter D_{84} in Eq. 2). Calibration with the Wilcock et al. flume data gave:

$$\zeta(\tau^*, F_s) = \left[1 + (0.15\sqrt{\frac{\tau_c^*}{\tau^*}} - 0.12)\ln(F_s)\right]^{10} \quad \text{for } \tau^*/\tau_c^* < 1.56 \quad (7)$$

$$\zeta(\tau^*, F_s) = 1 \quad \text{for } \tau^*/\tau_c^* > 1.56$$

where τ^* and τ_c^* were calculated with Eqs. 1 and 2 for $D_i = D_{84}$. This function performed as well as the Wilcock and Crowe equation for the bulk bedload transport when compared with the flume data of Wilcock et al., it produced results that are very similar to Figure 11 when compared with the field data, and gave a very similar result for α (i.e., linear variation with $<\tau^*>/<\tau_c^*>$) when used in the Monte Carlo approach. Consequently, it is not the Wilcock and

Crowe equation that should be questioned here, but the flume data from which it was derived: Are they representative of local transport in the field? Very precise local field measurements would be needed to confirm these results, not only for the bed shear stress and bedload transport, but also for the associated bed surface GSD (such data do not yet exist to the best of the author's knowledge).

A second question concerns the effects of the local bed morphology. The case of near-straight reaches was considered here, with no or little correlation between the depth and GSD. Developing probability functions that are typical of morphological units such as riffle, pools, and bars [*Buffington and Montgomery*, 1999b; *Bunte and Abt*, 2001] may necessitate a more sophisticated approach, linking these two parameters [*Ferguson*, 2003]. However, investigating the correlation between depth and grain size is challenged by uncertainties on the variance in GSDs, which may change with hydraulic roughness [*Buffington and Montgomery*, 1999a] or other external factors, such as the transport stage: The streambed textures are typically documented at low flow when the bed is at rest and likely reflect preferential transport by secondary flows, during hydrograph recession. For instance, there is no reason why the bed patchiness measured on the bed at rest would be representative of the bed during flooding.

To conclude, the investigation proposed in this paper considered variations around the mean input values, which themselves were assumed to be exact. However, an erroneous estimation of the width-averaged input data is likely to strongly impact the results. This aspect should be considered in further analysis. It should be noted that the Monte Carlo analysis can also be a useful tool for estimating the error on bedload prediction, with consideration of uncertainties attached to the measured (or estimated) field data [*Wilcock, et al.*, 2009].

CONCLUSIONS

Because they are nonlinear, bedload transport equations should logically under-predict

488 observed bedload transport when they are used with averaged (flow and bed) input data
489 [*Gomez and Church*, 1989; *Paola and Seal*, 1995; *Ferguson*, 2003; *Bertoldi, et al.*, 2009;
490 *Francalanci, et al.*, 2012]. However, this expectation has not been clearly demonstrated in
491 prior studies comparing predicted transport rates with observed values, which show over-
492 prediction, usually by several orders of magnitude [*Rickenmann*, 2001; *Barry, et al.*, 2004;
493 *Bathurst*, 2007; *Recking, et al.*, 2012].

494 In this paper, evidence of nonlinearity was shown by comparing 1D (flume-derived)
495 equations and 2D field measurements (Figure 10, Figure 11) and by comparing a 2D (field-
496 derived) equation with 1D flume measurements (Figure 14). Comparison with a 1D
497 nonthreshold equation derived for uniform sediments [*Recking*, 2010] and with no shear stress
498 correction produced under-prediction for low transport stages only (when $\tau^*/\tau_c^* < 1$), over-
499 prediction in the range $1 < \tau^*/\tau_c^* < 2$, and near adequate transport for higher transport stages
500 (Figure 10). Over-prediction in the range $1 < \tau^*/\tau_c^* < 2$ is typical of other 1D threshold
501 equations [*Recking, et al.*, 2012]. The nonthreshold fractional equation from Wilcock and
502 Crowe used with shear stress correction also under-predicted bedload for the low transport
503 stages (when $\tau^*/\tau_c^* < 1$) as expected by nonlinearity effects, and adequately reproduced
504 bedload for higher transport stages (Figure 11). On the other hand, the field-derived 2D
505 equation [*Recking*, 2013] that implicitly takes into account the variance in flow and bed
506 parameters correctly predicted the field data but over-predicted 1D bedload transport
507 measured in the flume by *Wilcock et al.* [2001] (Figure 14).

508 Under-prediction exists because each bedload data is by construction the average of
509 several local bedload values containing the variance in shear stress and bed GSD, whereas
510 such variance is absent from the mean input values used in bedload equations. The GSD was
511 reduced to three parameters (F_s, D_{50}, D_{84}/D_{50}) and probability distribution functions were
512 proposed to describe the variance associated with the flow and the bed. Then the Wilcock and

513 Crowe equation was compared with the field bedload data in a Monte Carlo approach, in
514 order to calibrate the parameters of these functions. The conclusion is that bedload prediction
515 is weakly sensitive to the variance in bed GSDs but is highly sensitive to the variance in shear
516 stress (Figure 19). The shear stress was modeled by a gamma function, whose shape
517 coefficient was found to vary linearly with the transport stage $<\tau^*>/<\tau_c^*>$. The variance in
518 shear stress suggests that local shear stress can exceed the critical shear stress for the bed
519 armor even for very low flow conditions (Figure 21); this may explain local armor break-up
520 and why the bedload GSD is frequently equivalent to the subsurface GSD (much finer than
521 the surface GSD).

522 Several aspects of this study remain to be investigated. In particular, little is known
523 about the variance in GSDs for a given reach, and new data (collected in the flume or in the
524 field) are needed for comparison with the Wilcock et al. [2001] data used here as
525 representative of 1D transport.

526

ACKNOWLEDGMENTS

This study was supported by Irstea and the ANR GESTRANS project granted to the author. It would not have been possible without the USDA and the USGS data sets, as well as all the other published data sets presented in Recking [2010]. The author is particularly grateful to Mary-Ann Madej from the USGS, Randy Klein from Redwood National and State Parks, Dieter Rickenmann from WSL, Mike Church from UBC, Ian Reid from Loughborough University, Sandra E. Ryan-Burkett from the US Forest Service, John Pitlick from Boulder University, and François Métivier from IPGP for having generously and spontaneously agreed to share their data. The author would also like to thank Rob Ferguson, Mike Church and other anonymous reviewers who greatly contributed to this paper by providing helpful reviews of an earlier version of this manuscript. Thanks are extended to John Buffington (Associate Editor), who contributed to this paper by providing additional reviews. Special thanks are addressed to John Pitlick for discussions and very helpful comments.

FIGURE CAPTIONS

Figure 1: Schematic representation of nonlinearity effects on a river cross section. Figure 1a illustrates a river section, its averaged parameters $<\tau^*>$ and $q_s(<\tau^*>)$, and its decomposition in local values τ_i^* and $q_s(\tau_i^*)$; Figure 1b indicates that the higher the value of the shear stress exponent, the greater the nonlinearity effects.

Figure 2: Cumulative distribution of $<D_{84}>$, slope $<S>$, and width $<W>$, for the field data set (109 reaches)

Figure 3: Variation of the slope $<S>$ with $<D_{84}>$ deduced from the field database

Figure 4: Grain size distributions for the field data set: (a) a selection of 78 GSDs from gravel bed rivers; (b) additional data (43 GSDs) including sand bed rivers

Figure 5: Plot of the sand fraction F_s as a function of the bed surface D_{84}

Figure 6: D_{84}/D_{50} ratio measured for a selection of 170 river reaches (left) and associated probability distribution function (right)

Figure 7: Relationship between the transport stage $<\tau^*>/<\tau c^*>$ and the bed surface $<D_{84}>$ and the slope $<S>$

Figure 8: Transport rates plotted as a function of the transport stage $<\tau^*>/<\tau c^*>$; (a) unit transport $<q_s>$ (g/s/m); (b) dimensionless transport (Einstein parameter $<\Phi>$)

566 Figure 9: Comparison of the *Wilcock et al.* [2001] data ($q_{s\ meas}$) with the *Recking* [2010]
567 equation ($q_s(<\tau^*>)$; Appendix B1), which represents a best fit of flume data having near-
568 uniform sediments
569
570 Figure 10: Comparison of the field data ($q_{s\ meas}$) with the *Recking* [2010] equation ($q_s(<\tau^*>)$;
571 Appendix B1), which represents a best fit of flume data having near-uniform sediments:
572 measured unit bedload $q_{s\ meas}$ vs. computed value $q_s <\tau>$ (left panel), and $q_{s\ meas} / q_s<\tau>$ ratio
573 vs. transport stage (right panel).
574
575 Figure 11: Comparison of the field data ($q_{s\ meas}$) with the Wilcock and Crowe equation [2003]
576 ($q_s(<\tau^*>)$; Appendix B2): measured unit bedload $q_{s\ meas}$ vs. computed value $q_s <\tau>$ (left panel),
577 and $q_{s\ meas} / q_s<\tau>$ ratio vs. transport stage (right panel).
578
579 Figure 12: Comparison of the field data (qs meas) with the field equation [*Recking*, 2010;
580 2013] (qs($<\tau^*>$); Appendix B3): measured unit bedload $q_{s\ meas}$ vs. computed value $q_s <\tau>$ (left
581 panel), and $q_{s\ meas} / q_s<\tau>$ ratio vs. transport stage (right panel).
582
583 Figure 13: Performance of the field equation *[Recking,* 2013; Appendix B3] across a broad
584 range of grain size and channel morphology
585
586 Figure 14: Comparison of the *Wilcock et al.* [2001] data (qs meas) with the field equation
587 [*Recking*, 2010; 2013] (qs($<\tau^*>$); Appendix B3); Fs is the sand fraction at the bed surface
588
589 Figure 15: Gamma function of $\tau/<\tau>$ plotted for different values of the shape parameter α
590

591 Figure 16: Modeling of GSD: (a) model comparison with three GSDs and difference between
592 computed and measured GSDs of (b) Figure 4a (78 GSDs) and (c) Figure 4b (43 GSDs)
593
594 Figure 17: Normal distribution of $D_{50}/<D_{50}>$ plotted for different values of the standard
595 deviation σ
596
597 Figure 18: Beta function of F_s plotted for different values of the shape parameters x_1 and x_2
598
599 Figure 19: Comparison of the results of the Monte Carlo simulation (curves) with the Figure
600 11b data (Box plots), for (a) constant α-values; (b) transport state-dependent α and several
601 values of $<D_{50}>$; (c) several combinations of α, σ_D, and x_1 with $\langle \tau^* \rangle / \langle \tau_c^* \rangle$, $<D_{84}>$ and $<S>$
602 linked by relationships illustrated in Figure 3 and Figure 7.
603
604 Figure 20: Bedload computation with the *Wilcock and Crowe* [2003] equation with and without
605 taking into account the variance in bed and flow parameters ($q_s(\tau)$ and $q_s(<\tau>)$, respectively):
606 example of the Lochsa River
607
608 Figure 21: Distribution of local transport stages τ/τ_c, for different mean transport stages
609 $<\tau>/<\tau_c>$
610
611
612
613

NOTATIONS

d	Flow depth [m]
D_x	Grain diameter (subscript denotes % finer) [m]
F_s	Sand fraction at the bed surface [-]
$< P >$	Width averaged value of parameter P: $< P >= \frac{1}{W}\int_{y=0}^{W} P dy$
Q	Flow discharge [m^3/s]
q	Specific discharge ($q=Q/W$) [$m^3/s/m$]
Q_s	Sediment discharge at equilibrium flow condition [kg/s]
q_s	Bedload transport rate per unit width ($q_s=Q_s/W$) [kg/s/m]
R	Hydraulic radius [m]
S	Slope [m/m]
s	Relative density ($s=\rho_s/\rho$) [-]
U	Vertically averaged flow velocity [m/s]
u^*	Shear velocity: $u^* = \sqrt{\tau/\rho}$ [m/s]
W	Channel width [m]
x_1, x_2	Parameters of the beta distribution for F_s
α	Parameter of the gamma function for τ
ξ	Coefficient in $\alpha=\xi<\tau^*>/<\tau c^*>$
σ_D	Standard deviation of the normal distribution for D_{50}
σ_{DR}	Standard deviation of the normal distribution for D_{84}/D_{50}
Φ	Dimensionless transport rate: $\Phi=q_{sv}/[g(s\text{-}1)D^3]^{0.5}$ [-]
ρ	Fluid density [kg/m^3]
ρ_s	Sediment density [kg/m^3]
τ	Bed shear stress [N/m^2]

638 τ^* Shields parameter calculated for diameter D_x [ ]: $\tau^*_x = \tau/[(\rho_s-\rho)gD_x]$ [-]

639 τ^*_c Critical Shields stress corresponding to grain entrainment [-]

640

APPENDIX

Appendix A: Main characteristics of the additional data

Site	Data source	Measurement technique*	W (m)	S ($x10^3$)	Q (m3/s)	U (m)	d (m)	D_{50}** (mm)	D_{84}** (mm)	Nb of values
Mondego River	Da Cunha [1969] in Brownlie, 1981	No information	*70–189*	*0.54–0.97*	*29–660*	*NA*	*0.45–2.45*	*2.2–2.6*	*4.7–6*	*219*
Mountain Creek	Einstein [1944] in Brownlie [1981]	Sediment discharge measured by trapping sediment in a mesh-covered hopper and pumping it into a weighing tank. Continuous water stage record. Discharge calculated from velocity (and depth) determined by means of floats.	*3.3–4.3*	*1.36–3.15*	*0.1–1.5*	*NA*	*0.04–0.44*	*0.3–0.9*	*0.4–1.7*	*100*
Saskatchewan River	Samide [1971] in Brownlie [1981]	Basket-type bed-load samplers, local velocity and depth measurements	*3–6.1*	*1.53–7.45*	*4.7–39.1*	*NA*	*0.73–2.74*	*1.5–7.5*	*22.8–178*	*55*
Hii River	Shinohara and Tsubaki [1959] in Brownlie [1981]	No information	*0.8–8*	*0.84–1.72*	*0.05–4.9*	*NA*	*0.11–0.73*	*1.3–1.5*	*2.7–3.2*	*23*
Nile River	Gaweesh and Van Rijn [1994]; Abdel-Fattah et al. [2004]	Nozzle (width = 0.096 m; height = 0.055 m; length = 0.085 m; rear width = 0.105 m; rear height = 0.06 m) connected to a nylon bag with a mesh size of 150 or 250 10^{-6}m. Velocity and depth measurements.	*200–578*	*0.04–0.09*	*NA*	*0.4–0.9*	*2.76–5.72*	*0.3–0.6*	*0.3–1.7*	*29*
Rhine River	Gaweesh and Van Rijn [1994]	Same as Nile River	*300–350*	*0.08–0.11*	*NA*	*0.5–1.3*	*4.5–7.4*	*0.9*	*1.9*	*12*
Turkey brook at Birkie Reach	Reid and Frostick [1986]	Three independent pit traps	*3*	*2.6–16.2*	*0.1–13.8*	*NA*	*0.064–0.93*	*22*	*42*	*206*
SF Cache la Poudre	Ryan et al [2005]	Helley-Smith sampler, velocity with Price AA or current meter	*7.3–15.1*	*7*	*0.5–16.6*	*0.33–1.73*	*0.16-0.64*	*68*	*115*	*89*
Cache Creek	Ryan et al [2005]	Same as SF Cache la Poudre	*5.1–5.3*	*21*	*0.7–2.7*	*0.5–1.1*	*0.30-0.48*	*46*	*115*	*60*
Coon Creek	Ryan et al [2005]	Same as SF Cache la Poudre	*4.5–6.7*	*31*	*0.3–4*	*0.5–1.7*	*0.15-0.39*	*83*	*215*	*88*
East Fork Encampt.	Ryan et al [2005]	Same as SF Cache la Poudre	*3.9–6.5*	*38*	*0.1–2.2*	*0.3–1.14*	*0.10-0.34*	*50*	*133*	*84*
Halfmoon Creek	Ryan et al [2005]	Same as SF Cache la Poudre	*8.3–9.6*	*9.2–16*	*0.5–10.8*	*0.35–1.75*	*0.16-0.59*	*62*	*108*	*155*
East Fork San Juan	Ryan et al [2005]	Wading version of an Elwha	*15–17.2*	*8*	*2.8–13.8*	*0.71–1.59*	*0.27-0.52*	*50*	*112*	*77*

		bedload sampler, 102×203mm							
Mid Fork Piedra	Ryan et al [2005]	Same as East Fork SJ	*11.4–13.8*	*9–19*	*1–10.9*	*0.45–1.63*	*0.19-0.53*	*80*	*210*	*86*
Silver Creek	Ryan et al [2005]	Same as East Fork SJ	*3.8–4.4*	*45*	*0.1–1.4*	*0.08–0.39*	*0.11-0.32*	*31*	*73*	*57*
Upper Florida	Ryan et al [2005]	Same as East Fork SJ	*11.3–17*	*1.2–15.1*	*1.1–15.3*	*0.27–1.35*	*0.41-0.89*	*210*	*550*	*37*
Redwood at Orick	Madej and Ozaki [1996] and unpublished USGS data	Qs (Helley-Smith sampler) and Q measured at Orick gauging station. W(Q), D_{50} and D_{84} from unpublished data	*11.7–70*	*1.4*	*1.8–569*	*NA*	*NA*	*5*	*18*	*221*
Fraser river at Agassiz	McLean et al [1999], Ferguson and Church [2009]	Basket sampler (610×255 mm) for high flows (>7000 cm) and half-size VuV sampler (225×115 mm) for lower flows. Discharge measured at gauging station.	*510*	*0.46*	*1085–11445*	*NA*	*NA*	*42*	*70*	*76*
Harris Cr.	Church and Hassan [2002]; Hassan and Church [2001]; Sterling and Church [2002]	Sediment trap	*15*	*13*	*4.2–18.4*	*NA*	*NA*	*70*	*100*	*22*
Tordera River	García and Sala [1998], Garcia et al [2000]	Pit trap	*5.5*	*20*	*2–7.5*	*0.9–1.63*	*0.27-0.45*	*50*	*170*	*220*
Bridge Cr.	Nanson [1974]	Basket sampler 38 cm long/30 cm wide, mesh size 6.4 mm, current meter and water stage recorder	*2.3*	*67*	*0.3–1.1*	*NA*	*NA*	*30*	*63*	*18*
Virginio Cr.	Tacconi and Billi [1987], Cencetti et al.,[1994]	Vortex tube Bedload values deduced from graph reading	*12*	*8*	*0.6–7.1*	*NA*	*NA*	*27*	*55*	*99*
Fall River FR1	Pitlick [1993].	Helley-Smith 76 mm, water stage record and calibration with a current meter	*9*	*3.2*	*0.92–10.71*	*0.34–1.37*	*0.30-0.87*	*11*	*20*	*175*
Fall River FR2	Pitlick [1993]	Same as FR1	*7*	*1.5*	*1.13–9.97*	*0.44–1.11*	*0.36-1.39*	*1*	*3*	*182*
Torrent Saint-Pierre (braided river)	Meunier et al [2006]	U with propeller CM OTT, HS 15*15cm, Net mesh 0.25mm.	*9.2-11*	*25*	*0.05-0.91**	*0.48-1.98*	*0.08-0.98*	*21*	*80*	*224*

642 *Discharge per unit width q [m^3/s/m] ** Measured at the bed surface
643

644 **Appendix B1: 1D Equation for uniform sediments (Recking, 2010)**

$$\Phi = 0.00005\left(\frac{\tau^*}{\tau_c^*}\right)^{12.9} \quad \text{for } \tau^*/\tau_c^* < 2.3S^{0.08} \tag{B1}$$

$$\Phi = 14\tau^{*2.5} \quad \text{for } \tau^*/\tau_c^* > 2.3S^{0.08}$$

645 With $\Phi = \frac{q_s}{\rho_s\sqrt{g(s-1)D_{50}^3}}$, $\tau_c^* = 0.15S^{0.275}$

646

647 **Appendix B2: Wilcock and Crowe [2003] bedload equation**

$$W_i^* = \begin{cases} 0.002\phi^{7.5} & for \quad \phi < 1.35 \\ 14\left(1-\frac{0.894}{\phi^{0.5}}\right)^{4.5} & for \quad \phi \geq 1.35 \end{cases} \tag{B2}$$

648 With

649 $W_i^* = \frac{(s-1)gq_{bi}}{f_i u_*^3}$ and $\phi = \frac{\tau}{\tau_{ri}}$

650 $\tau = 17\left(SD_{65}\right)^{1/4}U^{3/2}$ (D_{65} in mm)

651 $\tau_{ri} = \tau_{r50}\left(\frac{D_i}{D_{s50}}\right)^b$

652 $b = \frac{0.67}{1+\exp\left(1.5-\frac{D_i}{D_{sm}}\right)}$

653 $\tau_{rm} = (s-1)\rho g D_{sm}(0.021+0.015\exp[-20F_s])$

654 Where q_{vi} is the volumetric transport rate of size i per unit width ($q_v=\Sigma q_{vi}$), D_{sm} is the
655 geometric mean particle diameter of the bed surface and F_s is the sand fraction at the bed
656 surface.
657

658 **Appendix B3: Recking (2013)**

$$\Phi(\tau^*) = 14\tau_{D84}^{*2.5}/[1+(\tau_m^*/\tau_{D84}^*)^4] \tag{B3}$$

659 With $\Phi = \frac{q_s}{\rho_s\sqrt{g(s-1)D_{84}^3}}$, $\tau_m^* = (5S+0.06)\left(D_{84}/D_{50}\right)^{4.4\sqrt{S}-1.5}$ for gravel and 0.045 for sand.

660 $\tau_{D84}^*(R)=RS/[(s\text{-}1)D_{84}]$ or $\tau_{84}^*(q) = \frac{S}{(s-1)D_{84}[2/W+74p^{2.6}(gS)^p q^{-2p}D_{84}^{3p-1}]}$

661 where $q = Q/W$ and where $p = 0.23$ when $q/\sqrt{gSD_{84}^3} < 100$ and $p = 0.3$ otherwise.

TABLES

Run	Fs* (x100)	D_{50}* (mm)	D_{84}* (mm)	Slope (x10^3)	q (m²/s)	d (m)	q_s (g/m/s)
BOMC	37.9-59.6	0.5-2.8	8-14.9	0.6-16.2	0.029-0.095	0.09-0.12	0.002-572
J27	15.5-27.7	4-5.5	16.4-20.2	2.1-17	0.05-0.13	0.09-0.11	0.003-779
J21	3.4-16.5	5.5-8	18-21.8	3.3-18.5	0.065-0.126	0.1-0.12	0.017-152
J14	0.6-1.8	9-12	21.4-23.2	5.2-18.6	0.079-0.133	0.102-0.12	0.019-115
J06	0-0.3	10.5-12.9	20.4-24.8	4.5-22.5	0.078-0.133	0.1-0.11	0.000-204

* measured at the bed surface

Table 1: Experimental runs from Wilcock et al 2001

Parameter	Range
Slope (m/m)	0.00004–0.085
Diameter D_{50} (mm)	0.25–220
Diameter D_{84} (mm)	0.3–558
Bankfull depth (m)	0.04–7.5
Bankfull width (m)	0.3–578

Table 2: Main characteristics of field data

Class	*i* (%)	D_i (mm)	C_n	*Remark*
0	$100F_s$	D_m	-	D_m = 2mm but if F_s = 0 D_m = the minimum diameter of the GSD
1			16	
2	$\frac{50-100F_s}{C_n}+100F_s$	$\frac{D_{50}-D_m}{C_n}+D_m$	3.3	3.3 replaced by 8 if D_m > 2 mm
3			1.9	
4			1.3	
5	50	D_{50}	-	
6	60	$\frac{D_{84}-D_{50}}{C_n}+D_{50}$	5.9	
7	70		2.3	
8	84	D_{84}	-	
9	90		1.3	
10	98	C_nD_{84}	2.5	2.5 replaced by 1.5 if D_m > 2 mm
11	100		5.1	

Table 3: Grain Size distribution Model. Input data are D_{50}, D_{84}, F_s (the sand fraction), and D_m if Fs=0 (minimum grain size). C_n is a coefficient and D_i is the upper limit of the size class. For constructing a GSD, Fs and C_n are used for computing the limits of each size class (column 3) and the % in each class (column 2).

685 **REFERENCES**

686 Abdel-Fattah, S., A. Amin, and L. C. Van Rijn (2004), Sand transport in Nile river, Egypt,
687 *journal of Hydraulic Engineering*, *130*, 488-500.
688 Andrews, E. D. (1983), Entrainment of gravel from naturally sorted riverbed material,
689 *Geological Society of America Bulletin*, *94*, 1225-1231.
690 Barkett, B. L. (1998), The relationship between grain size and shear stress in two gravel bed
691 streams, Univ. of Colo., Boulder, CO.
692 Barry, J. J., J. M. Buffington, P. Goodwin, J. G. King, and W. W. Emmett (2008),
693 Performance of bedload transport equations relative to geomorphic significance: predicting
694 discharge and its transport rate, *Journal of Hydraulic Engineering (ASCE)*, *134*, 601-615.
695 Barry, J. J., J. M. Buffington, and J. G. King (2004), A general power equation for predicting
696 bed load transport rates in gravel bed rivers, *Water Resources Research*, *40*, 1-22.
697 Barry, J. J., J. M. Buffington, and J. G. King (2007), Correction to "A general power equation
698 for predicting bed load transport rates in gravel bed rivers", *Water Resources Research*, *43*.
699 Bathurst, J. C. (2007), Effect of coarse surface layer on bed-load transport, *Journal of*
700 *Hydraulic Engineering (ASCE)*, *133*, 1192-1205.
701 Bertoldi, W., P. Ashmore, and M. Tubino (2009), A method for estimating the mean bed load
702 flux in braided rivers, *Geomorphology*, *103*, 330-340.
703 Brownlie, W. R. (1981), Computation of alluvial channel data: Laboratory and Field, 213 pp,
704 California Institute of Technology, Passadena, California.
705 Buffington, J. M. (2000), The legend of A. F. Shields (Closure), *Journal of Hydraulic*
706 *Engineering*, *126*, 721-723.
707 Buffington, J. M. (2012), Changes in channel morphology over human time scales, in *Gravel-*
708 *bed Rivers: Processes, Tools, Environments*, edited by M. Church, Biron, P.M., Roy, A.G.
709 (Eds.),, pp. 435–463., Wiley, Chichester, UK.
710 Buffington, J. M., and D. R. Montgomery (1997), A systematic analysis of eight decades of
711 incipient motion studies, with special reference to gravel-bedded rivers, *Water Resources*
712 *Research*, *33*, 1993-2027.
713 Buffington, J. M., and D. R. Montgomery (1999a), Effects of hydraulic roughness on surface
714 textures of gravel-bed rivers, *Water Resources Research*, *35*, 3507.
715 Buffington, J. M., and D. R. Montgomery (1999b), A procedure for classifying textural facies
716 in gravel-bed rivers, *Water Resources Research*, *35*, 1903.
717 Bunte, K., and S. R. Abt (2001), Sampling surface and subsurface particle-size distributions
718 in Wadable and cobble bed streams for analyses in sediment transport, hydraulics and
719 streambed monitoring, 450 pp, USDA Report RMRS-GTR-74.
720 Cencetti, C., P. Tacconi, M. Del Prete, and M. Rinaldi (1994), Variability of gravel movement
721 on the Virginio gravel-bed stream (central Italy) during some floods, paper presented at
722 Variability in Stream Erosion and Sediment Transport (Proceedings of the Canberra
723 Symposium December 1994). IAHS Publ. no. 224.3-11
724 Chiari, M., and D. Rickenmann (2010), Back-calculation of bedload transport in steep
725 channels with a numerical model, *Earth Surface Processes and Landforms*, *36*, 805-815.
726 Church, M., and M. A. Hassan (2002), Mobility of bed material in Harris Creek, *Water*
727 *Resources Research*, *38*, 19-31.
728 Church, M., and R. Kellerhalls (1978), On the statistics of grain size variation along a gravel
729 bed river, *Can. J. Earth Sci.*, *15*, 1151-1160.
730 Church, M., and A. Zimmerman (2007), Form and stability of step-pool channels: Research
731 progress, *Water Resources Research*, *43*, 1-21.
732 Crowder, D. W., and P. Diplas (1997), Sampling heterogeneous deposits in gravel-bed
733 streams, *Journal of Hydraulic Engineering*, *123*, 1106-1117.

Da Cunha, L. V. (1969), River Mondego, Portugal," Personal Communication, Laboratorio Nacional De Engenharia Civil, Lisboa (Published in Peterson, A. W. , and Howells , R. F. , "A Compendium of Solids Transport Data for Mobile Boundary Channels," Report No. HY-1973-ST3, Department of Civil Engineering, University of A1 berta, Canada, January 1973). edited.

Dietrich, W. E., J. W. Kirchner, H. Ikeda, and F. Iseya (1989), Sediment supply and the development of the coarse surface layer in gravel-bedded rivers, *Nature*, *340*, 215-217.

Dietrich, W. E., P. A. Nelson, E. Yager, J. G. Venditti, M. P. Lamb, and L. Collins (2006), Sediment patches, sediment supply and channel morphology, in *In: River, Coastal and Estuarine: Morphodynamics,Parker, G., and Garcia, M. H. (Eds.), Taylor and Francis/Balkema, Lisse, The Netherlands*, edited, pp. 79-90.

Einstein, H. A. (1944), Bed Load Transportation in Mountain Creek," U.S. Soil Conservation Service, SCS-TP-55, 50pp.

Einstein, H. A. (1950), The bed-load function for sediment transportation in open channel flows, 71 pp, United States Department of Agriculture - Soil Conservation Service, Washington.

Ferguson, R. (2007), Flow resistance equations for gravel and boulder bed streams, *Water Resources Research*, *43*, 1-12.

Ferguson, R. (2012), River channel slope, flow resistance, and gravel entrainment thresholds, *Water Resour. Res.*, *48*, 1-13.

Ferguson, R., and M. Church (2009), A critical perspective on 1-D modeling of river processes: Gravel load and aggradation in lower Fraser River, *Water Resour. Res.*, *45*.

Ferguson, R. I. (2003), The missing dimension: effects of lateral variation on 1-D calculations of fluvial bedload transport, *Geomorphology*, *56*, 1-14.

Francalanci, S., L. Solari, M. Toffolon, and G. Parker (2012), Do alternate bars affect sediment transport and flow resistance in gravel bed rivers?, *Earth Surface Processes and Landforms*, *37*, 866-875.

Gaeuman, D., E. D. Andrews, A. Krause, and W. Smith (2009), Predicted fractional bed load transport rates: Application of the Wilcok-Crowe equations to a regulated gravel bed river, *Water Resour. Res.*, *45*, 1-15.

Garcia, C., J. B. Laronne, and M. Sala (2000), Continuous monitoring of bedload flux in a mountain gravel-bed river, *Geomorphology*, *34*, 23-31.

García, C., and M. Sala (1998), Application de formulas de transporte de fondo a un rio de gravas: comparacion con las tasas reales de transporte en el rio tordera, *Ingeniería del Agua*, *5*, 59-72.

Gaweesh, M. T. K., and L. C. Van Rijn (1994), Bed-load sampling in sand-bed rivers, *Journal of Hydraulics Engineering*, *120*, 1364-1384.

Gomez, B., and M. Church (1989), An assessment of bedload sediment transport formulae for gravel bed rivers, *Water Resources Research*, *25*, 1161-1186.

Habersack, H. M., and J. B. Laronne (2002), Evaluation and improvement of bed load discharge formulas based on Helley-Smith sampling in an Alpine gravel bed river, *Journal of Hydraulic Engineering*, *128*, 484-499.

Hassan, M. A., and M. Church (2001), Sensitivity of bed load transport in Harris Creek: Seasonal and spatial variation over a cobble-gravel bar, *Water Resources Research*, *37*, 813.

King, J. G., W. W. Emmett, P. Whiting, S. T. Kenworthy, and J. J. Barry (2004), Sediment transport data and related information for selected corse-bed streams and rivers in Idaho, (http://www.fs.fed.us/rm/boise/research/watershed/BAT/).

Lamb, M. P., W. E. Dietrich, and J.-G. Venditti (2008), Is the critical Shields stress for incipient sediment motion dependent on channel-bed slope?, *J. Geophys. Res.*, *113*.

Madej, M. A., and V. Ozaki (1996), Channel response to sediment wave propagation and movement, Redwood Creek, california, USA, *Earth Surface Processes and Landforms*, *21*, 911-927.

McLean, D. G., M. Church, and B. Tassone (1999), Sediment transport along lower Fraser River, 1, Measurements and hydraulic computations, *Water Resources Research*, *35*, 2533-2548.

Meunier, P., F. Metivier, E. Lajeunesse, A. S. Meriaux, and J. Faure (2006), Flow pattern and sediment transport in a braided river: The "torrent de St Pierre" (French Alps), *Journal of Hydrology*, *330*, 496-505.

Meyer-Peter, E., and R. Mueller (1948), Formulas for bed-load transport, paper presented at Procedings 2d Meeting IAHR, Stockholm.39-64

Montgomery, D. R., and J. M. Buffington (1997), Channel-reach morphology in mountain drainage basins, *Geological Society of America Bulletin*, *109*, 596-611.

Mueller, E. R., J. Pitlick, and J. M. Nelson (2005), Variation in the reference Shields stress for bed load transport in gravel-bed streams and rivers, *Water Resources Research*, *41*, W04006 (04001-04010).

Nanson, G. C. (1974), Bedload and suspended-load transport in a small, steep, mountain stream, *Am. J. Sci*, *274*, 471-486.

Nicholas, A. P. (2000), Modelling bedload yield in braided gravel bed rivers, *Geomorphology*, *36*, 89-106.

Paola, C. (1996), *Incoherent structures: turbulence as a metaphor for stream braiding*, 706-723 pp., In Ashworth, P.J., Bennet, S.J., Best, J.L., McLelland, S.J. (Eds), John Wiley and sons.

Paola, C., and R. Seal (1995), Grain size patchiness as a cause of selective deposition and downstream fining, *Water Resources Research*, *31*, 1395-1408.

Parker, G. (1978), Self-formed straight rivers with equilibrium bank and mobile bed. Part 2 : the gravel river, *Journal of Fluid mechanics*, *89*, 127-146.

Parker, G. (1990), Surface-based bedload transport relation for gravel rivers, *Journal of Hydraulic Research*, *28*, 417-428.

Parker, G. (2009), Transport of gravel and sediment mixtures, in *ASCE Manual 54 "Sedimentation Engineering"*, edited by ASCE.

Parker, G., and P. C. Klingeman (1982), On why gravel bed streams are paved, *Water Resources Research*, *18*, 1409-1423.

Parker, G., P. C. Klingeman, and D. G. McLean (1982), Bedload and size distribution in paved gravel-bed streams, *Journal of the Hydraulics Division (ASCE)*, *108*, 544-571.

Parker, G., G. Seminara, and L. Solari (2003), Bed load at low Shields stress on arbitrarily sloping beds: Alternative entrainment formulation, *Water Resources Research*, *39*, 1183.

Parker, G., P. R. Wilcock, C. Paola, W. E. Dietrich, and J. Pitlick (2007), Physical basis for quasi-universal relations describing bankfull hydraulic geometry of single-thread gravel bed rivers, *J. Geophys. Res.*, *112*, F04005.

Pitlick, J. (1993), Response and recovery of a subalpine stream following a catastrophic flood, *Geological Society of America Bulletin*, *105*, 657-670.

Pitlick, J., E. R. Mueller, C. Segura, R. Cress, and M. Torizzo (2008), Relation between flow, surface layer armoring and sediment transport in gravel bed rivers, *Earth Surface Processes and Landforms*, *33, DOI:10.1002/esp.1607*, 1192-1209.

Recking, A. (2009), Theoretical development on the effects of changing flow hydraulics on incipient bedload motion, *Water Resources Research*, *45, W04401*, 16.

Recking, A. (2010), A comparison between flume and field bedload transport data and consequences for surface based bedload transport prediction, *Water Resources Research*, *46*, 1-16.

833 Recking, A. (2012), Influence of sediment supply on mountain streams bedload transport
834 rates, *Geomorphology*, 12 p.
835 Recking, A. (2013), A simple method for calculating reach-averaged bedload transport,
836 *Journal of Hydraulic Engineering*, *139*.
837 Recking, A., P. Frey, A. Paquier, P. Belleudy, and J. Y. Champagne (2008), Feedback
838 between bed load and flow resistance in gravel and cobble bed rivers, *Water Resources*
839 *Research*, *44*, 21.
840 Recking, A., F. Liébault, C. Peteuil, and T. Jolimet (2012), Testing several bed load transport
841 equations with consideration of time scales, *Earth Surface Processes and Landforms*.
842 Reid, I., and L. E. Frostick (1986), Dynamics of bedload transport in Turkey Brook, a coarse-
843 grained alluvial channel, *Earth Surface Processes and Landforms*, *11*, 143-155.
844 Rickenmann, D. (2001), Comparison of bed load transport in torrents and gravel bed streams,
845 *Water Resources Research*, *37*, 3295.
846 Rickenmann, D., and A. Recking (2011), Evaluation of flow resistance in gravel-bed rivers
847 through a large field dataset, *Water Resources Research*, *47*, 1-22.
848 Ryan, S. E., L. Porth, and C. Troendle (2005), Coarse sediment transport in mountain streams
849 in Colorado and Wyoming, USA., *Earth Surface Processes and Landforms*, *30*, 269-288.
850 Ryan, S. E., L. S. Porth, and C. A. Troendle (2002), Defining phases of bedload transport
851 using piecewise regression, *Earth Surface Processes and Landforms*, *27*, 971-990.
852 Samide, G. W. (1971), Sediment transport measurements, PhD thesis dissertation, University
853 of Alberta.
854 Segura, C., J. H. McCutchan, W. M. Lewis, and J. Pitlick (2010), The influence of channel
855 bed disturbance on algal biomassin a Colorado muntain stream, *Ecohydrology*, 11.
856 Shinohara, K., and T. Tsubaki (1959), On the characteristics of sand waves formed upon beds
857 of the open channels and rivers, reports of Research I n s t i t u t e of Applied Mechanics,
858 Vol. V I I , No. 25, Kyushu University.
859 Sterling, M. S., and M. Church (2002), Sediment trapping characteristics of a pit trap and the
860 Helley-Smith sampler in a cobble gravel bed river, *Water Resour. Res.*, *38*, 1-19.
861 Tacconi, P., and P. Billi (1987), Bedload transport masurements by the vortex-tube trap on
862 Virginio Creek, Italy, in *Sediment transport in gravel bed rivers*, edited by C. R. Thorne,
863 Bathurst, J.C.,Hey, R.D., pp. 583-606, John Wiley & Sons Ltd, Chichester.
864 Tunnicliffe, J., M. Hicks, P. Ashmore, J. Walsh, J. T. Gardner, and M. Duncan (2012), Use of
865 2D hydraulic models to develop and improve parameterized 1D models of sediment transport
866 paper presented at EGU 2012 (Poster Session), Vienna, Austria
867 Wilcock, P., J. Pitlick, and Y. Cui (2009), Sediment transport primer, Estimating bed-material
868 transport in gravel-bed rivers, 78 pp, Gen Tech Rep RMRS-GTR-226. Fort Collins, CO: U.S.
869 Department of Agriculture, Forest service, Rocky Mountain Research Station.
870 Wilcock, P. R., and J. C. Crowe (2003), Surface-based transport model for mixed-size
871 sediment, *Journal of Hydraulic Engineering (ASCE)*, *129*, 120-128.
872 Wilcock, P. R., S. T. Kenworthy, and J. C. Crowe (2001), Experimental study of the transport
873 of mixed sand and gravel, *Water Resources Research*, *37*, 3349.
874 Wilcock, P. R., and B. W. McArdell (1993), Surface-based fractional transport rates:
875 Mobilization thresholds and partial transport of a sand-gravel sediment, *Water Resources*
876 *Research*, *29*, 1297-1312.
877 Wolman, M. G. (1954), Method of sampling coarse river bed material, *Transactions of the*
878 *American Geophysical Union,*, *35*, 951-956.
879
880

Recking, A. (2018), An analysis of nonlinearity effects in bed load transport prediction, J. Geophys. Res. Earth Surf., 118, doi:10.1002/jgrf.20090.

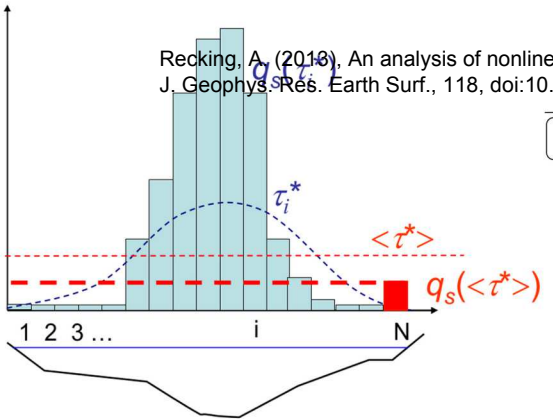

$$\langle \tau^* \rangle = \frac{1}{N} \sum_N \tau_i^*$$

$$q_s(\langle \tau^* \rangle) < \frac{1}{N} \sum_N q_s(\tau_i^*)$$

$$\frac{\left\langle \tau^* \right\rangle^p}{\left\langle \tau^* \right\rangle^p}$$

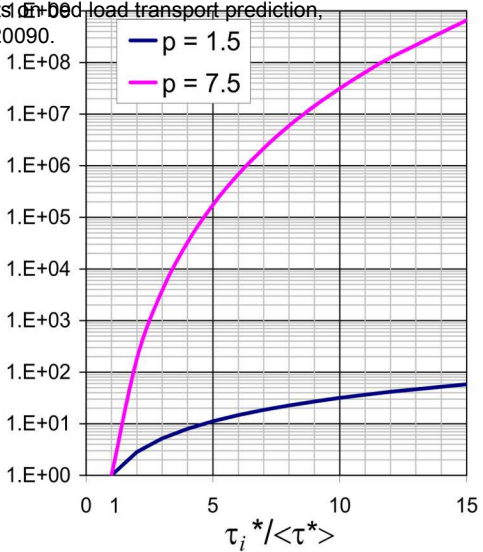

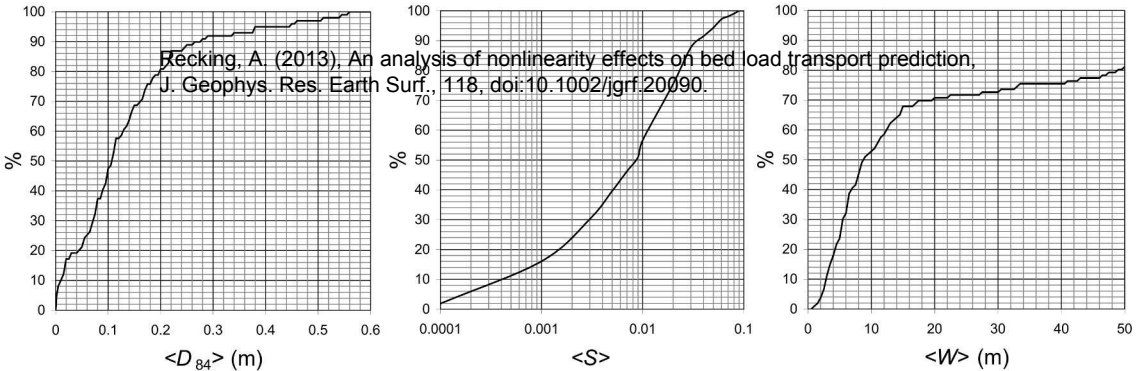
Recking, A. (2013), An analysis of nonlinearity effects on bed load transport prediction,
J. Geophys. Res. Earth Surf., 118, doi:10.1002/jgrf.20090.
%
<D 84> (m)
<S>
<W> (m)

2013), An analysis of nonlinearity effects on bed load transpo
Res. Earth Surf., 118, doi:10.1002/jgrf.20090.

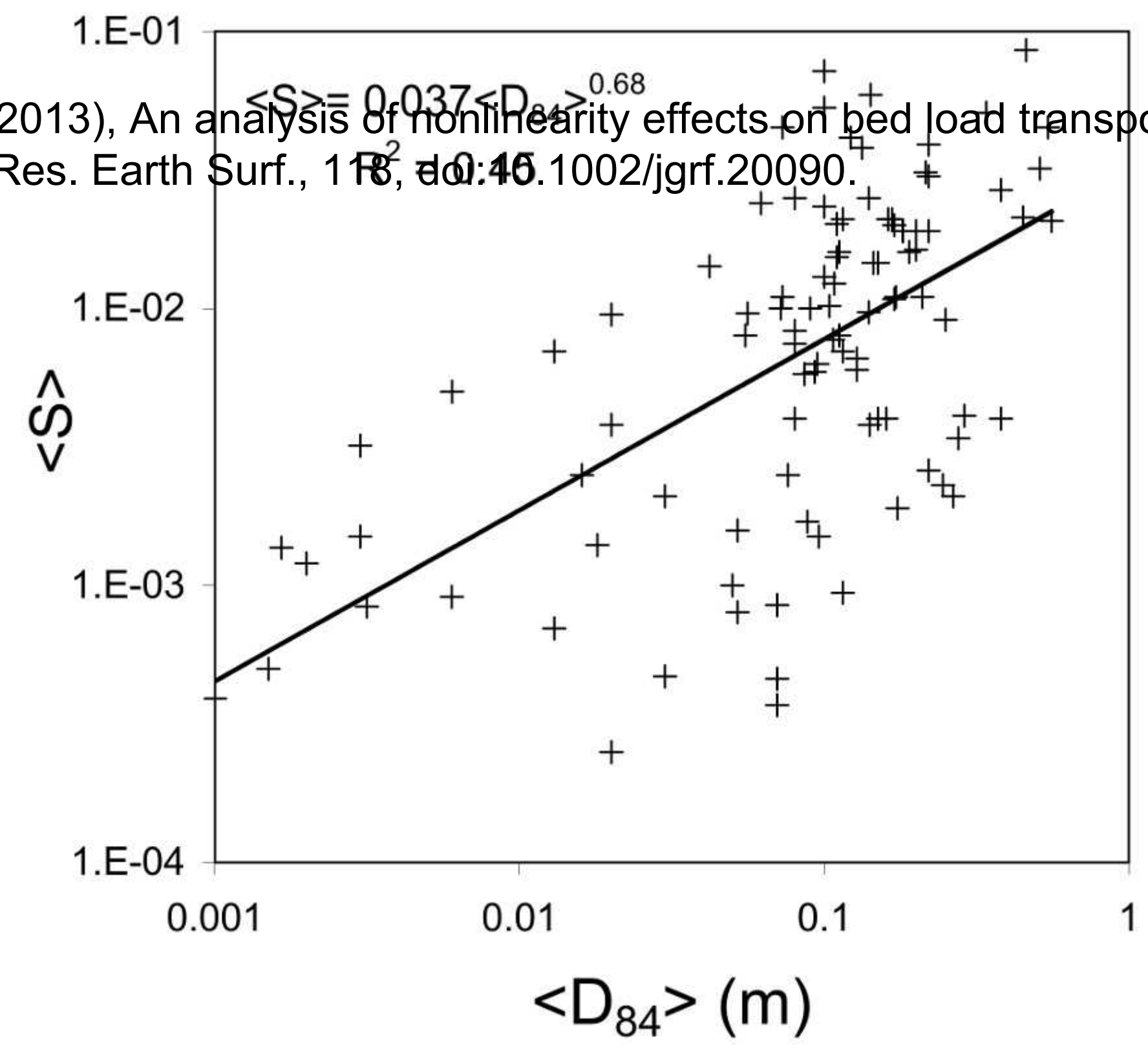

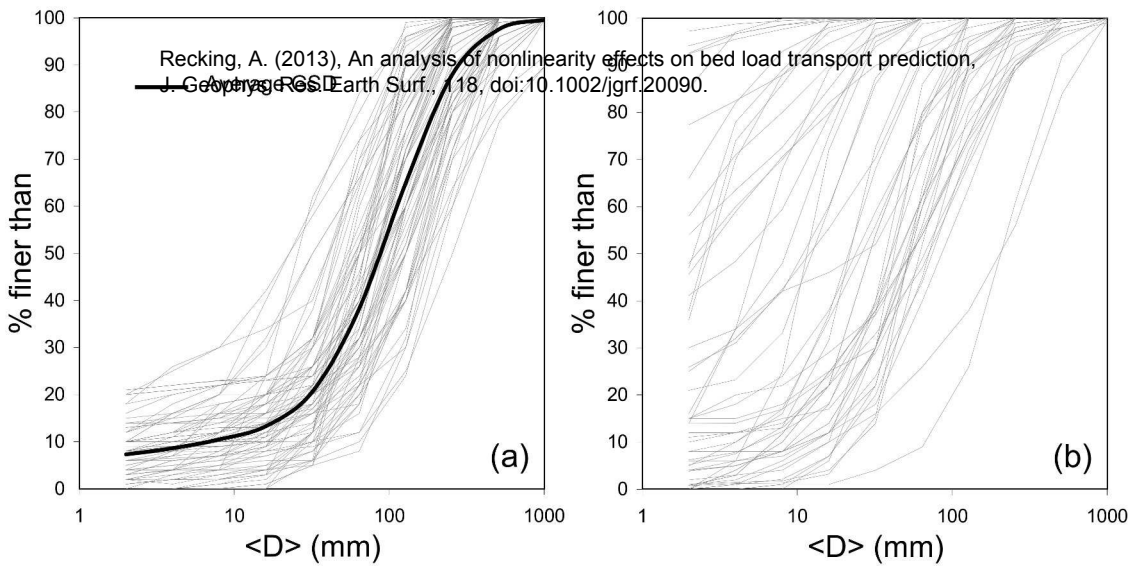
Recking, A. (2013), An analysis of nonlinearity effects on bed load transport prediction,
J. Geophys. Res. Earth Surf., 118, doi:10.1002/jgrf.20090.
Average PSD
% finer than
<D> (mm)
(a)
(b)

2013), An analysis of nonlinearity effects on bed load transpo
Res. Earth Surf., 118, doi:10.1002/jgrf.20090.

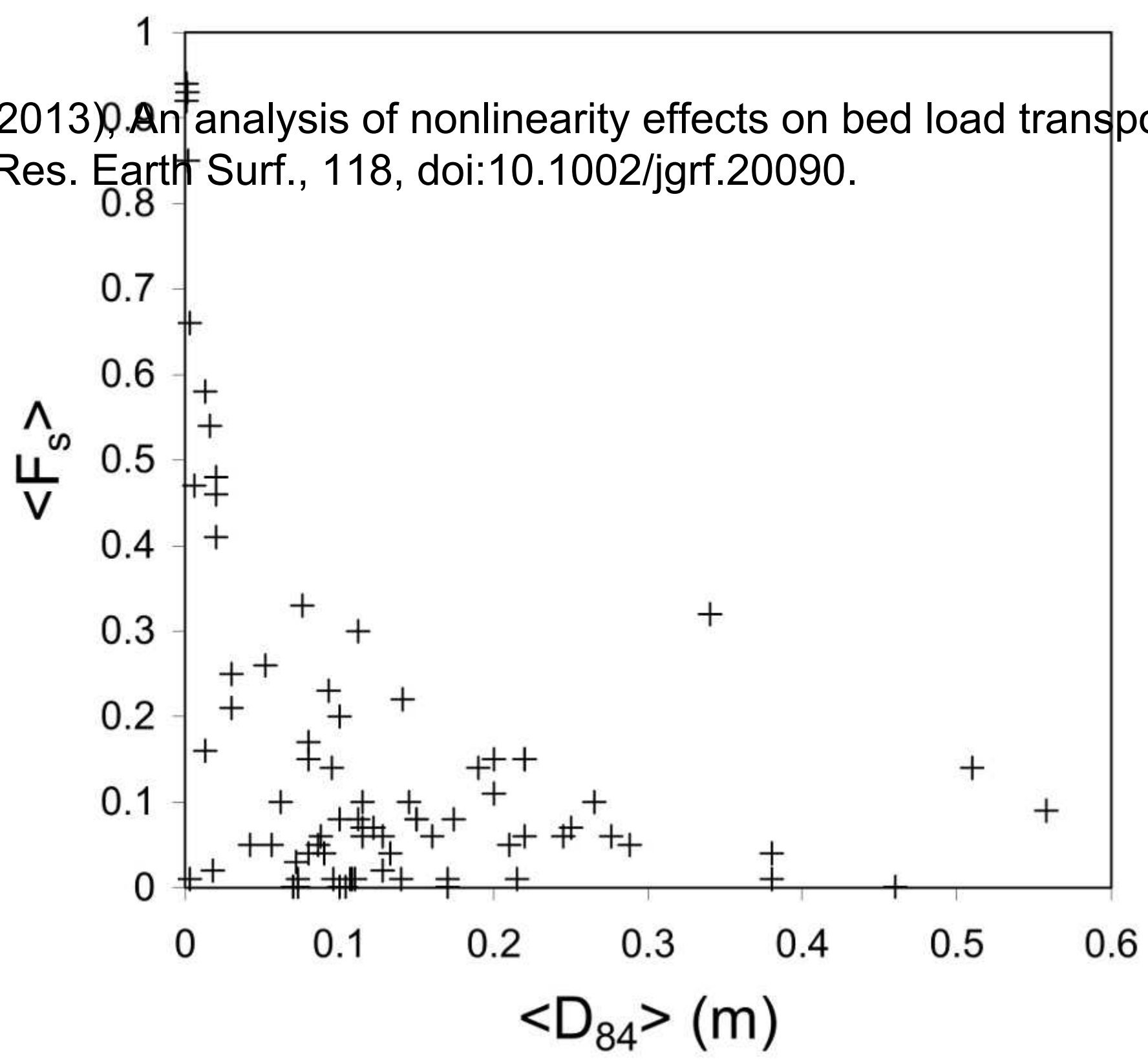

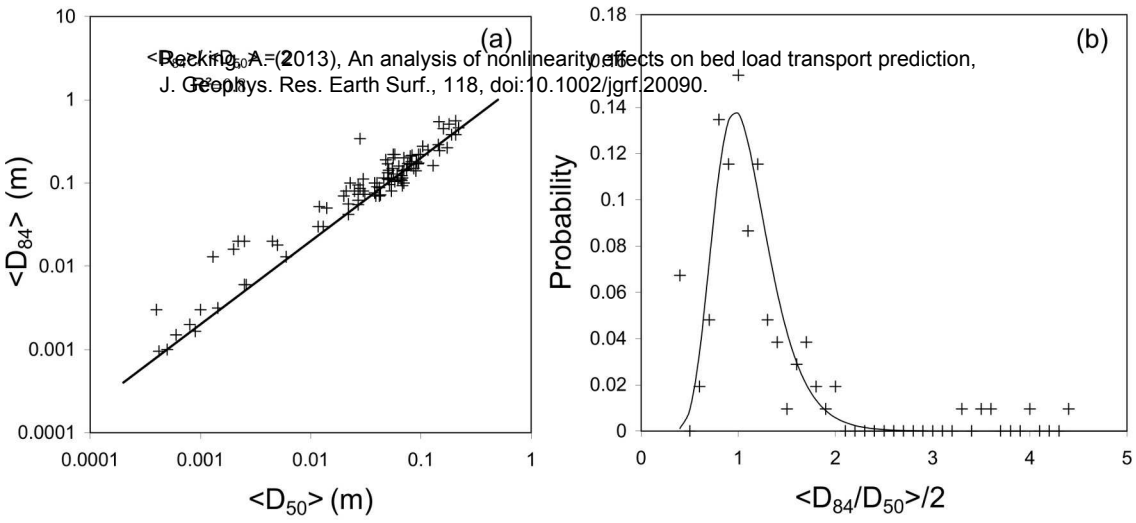

Recking, A. (2013), An analysis of nonlinearity effects on bed load transport prediction, J. Geophys. Res. Earth Surf., 118, doi:10.1002/jgrf.20090.

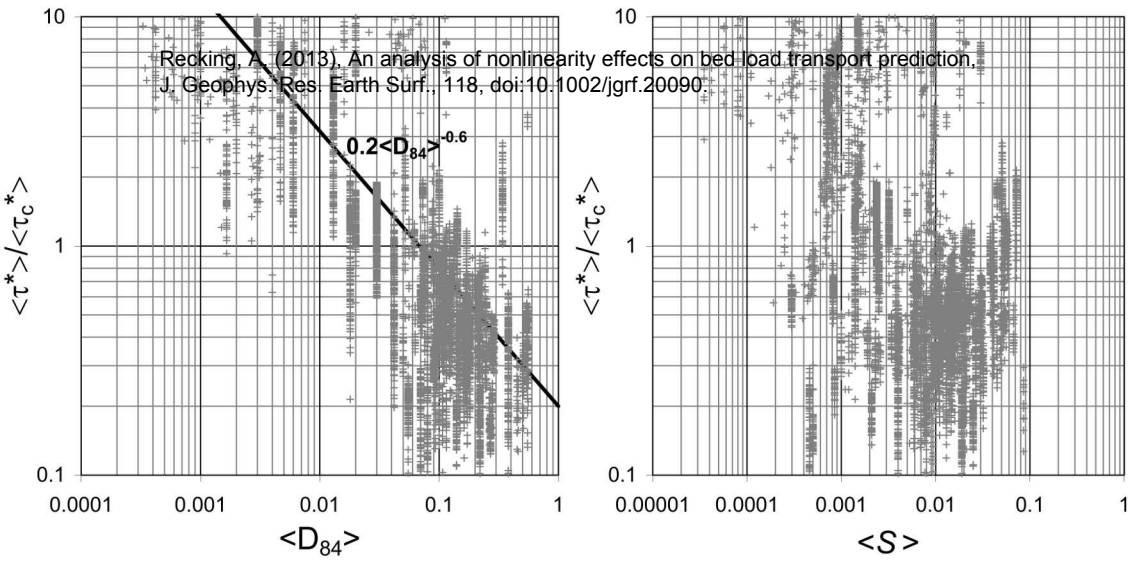
Recking, A. (2013), An analysis of nonlinearity effects on bed load transport prediction, J. Geophys. Res. Earth Surf., 118, doi:10.1002/jgrf.20090.
0.2<D84>-0.6
<τ*>/<τc*>
<D84>
<S>
10
1
0.1
0.0001
0.001
0.01
0.1
1
0.00001

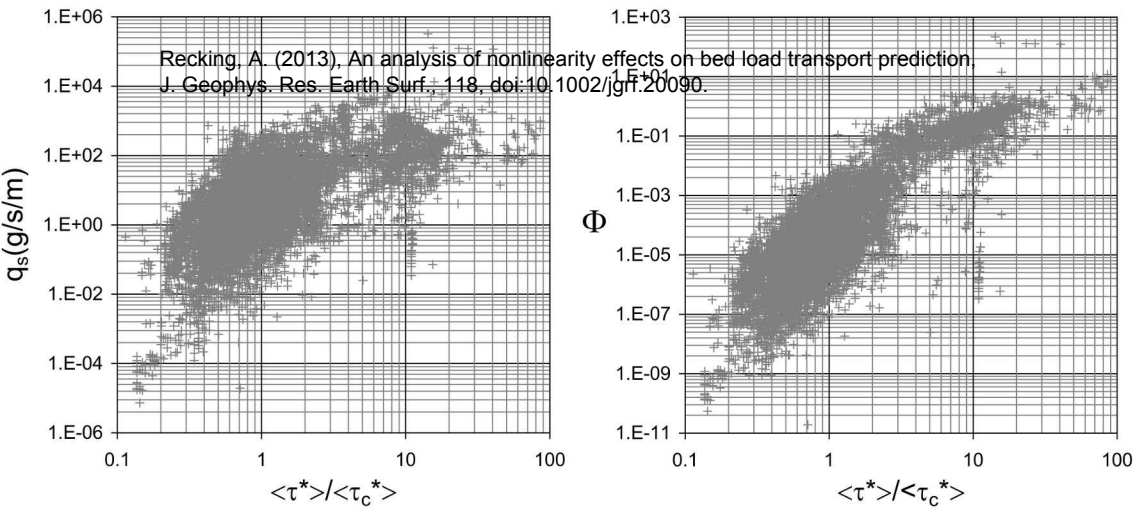
Recking, A. (2013), An analysis of nonlinearity effects on bed load transport prediction,
J. Geophys. Res. Earth Surf., 118, doi:10.1002/jgrf.20090.
1.E+06
1.E+04
1.E+02
1.E+00
1.E-02
1.E-04
1.E-06
q_s(g/s/m)
0.1
1
10
100
$<\tau^*>/<\tau_c^*>$
1.E+03
1.E+01
1.E-01
1.E-03
1.E-05
1.E-07
1.E-09
1.E-11
Φ
0.1
1
10
100
$<\tau^*>/<\tau_c^*>$

2013), An analysis of nonlinearity effects on bed load transpo
Res. Earth Surf., 118, doi:10.1002/jgrf.20090.

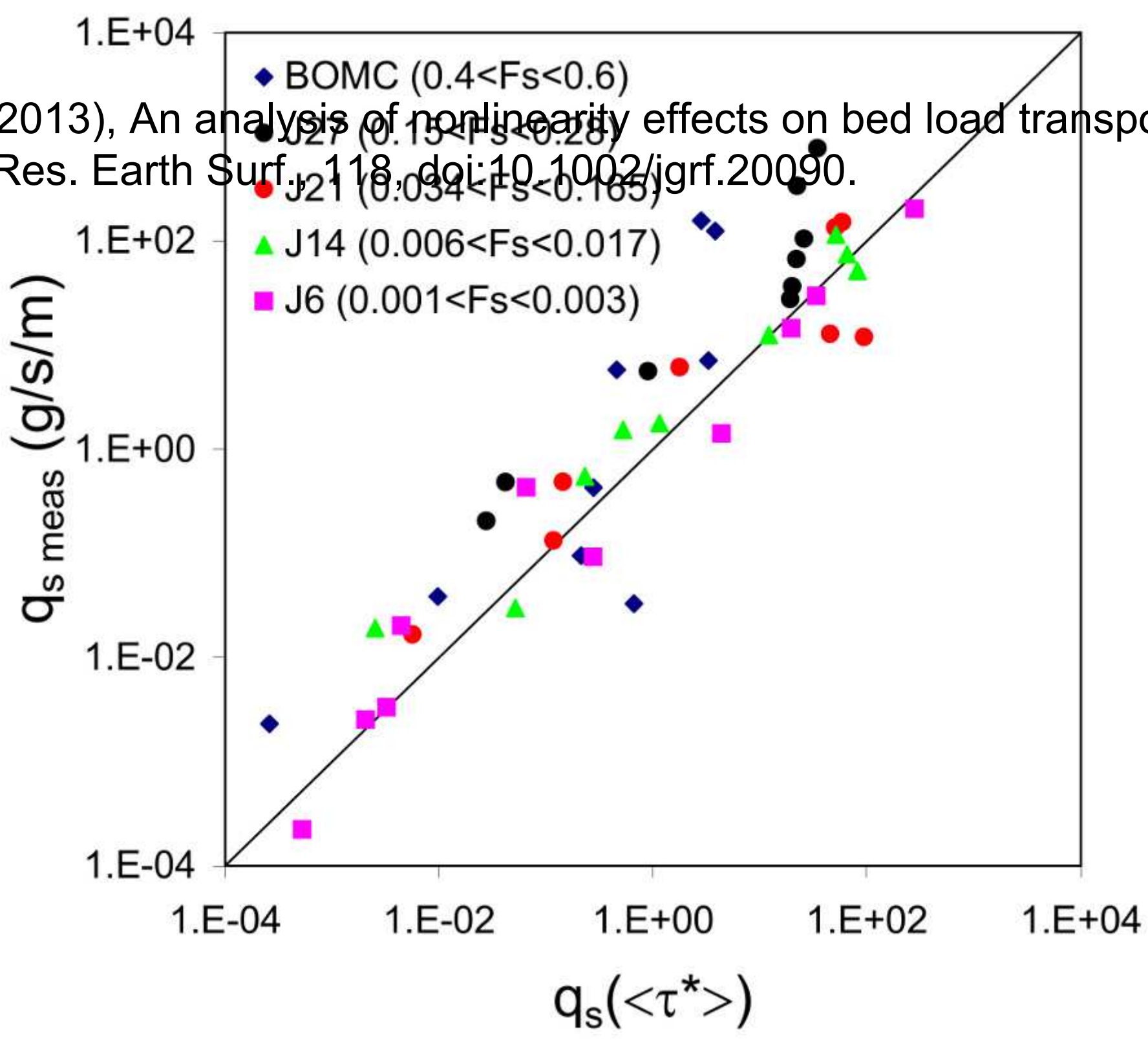

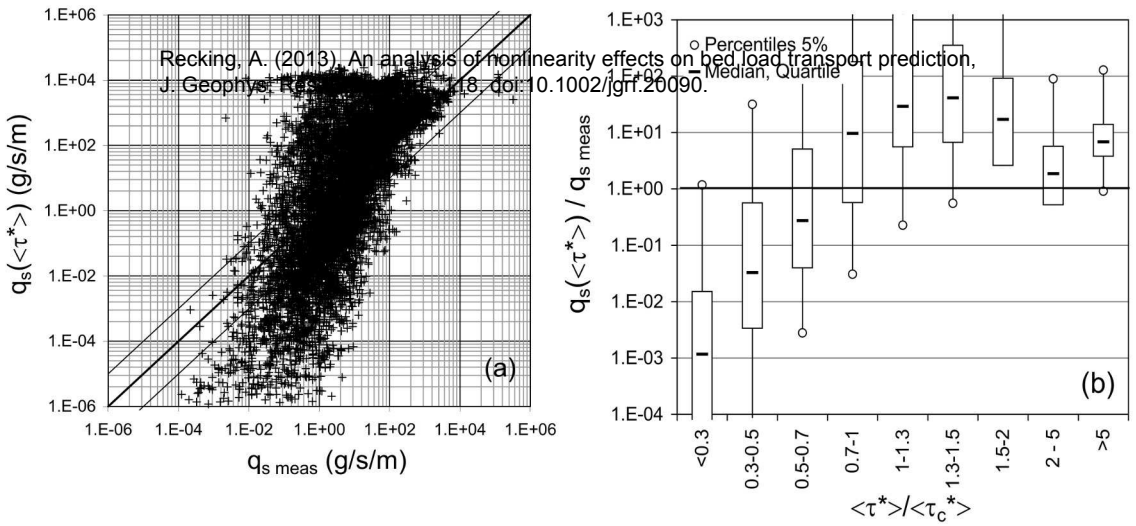
Recking, A. (2013), An analysis of nonlinearity effects on bed load transport prediction,
J. Geophys. Res.
118. doi:10.1002/jgrf.20090.
(a)
$q_s(<\tau^*>)$ (g/s/m)
$q_{s\ meas}$ (g/s/m)
1.E-06
1.E-04
1.E-02
1.E+00
1.E+02
1.E+04
1.E+06
(b)
Percentiles 5%
Median, Quartile
$q_s(<\tau^*>) / q_{s\ meas}$
1.E+03
1.E+01
1.E-01
1.E-02
1.E-03
1.E-04
<0.3
0.3-0.5
0.5-0.7
0.7-1
1-1.3
1.3-1.5
1.5-2
2 - 5
>5
$<\tau^*>/<\tau_c^*>$

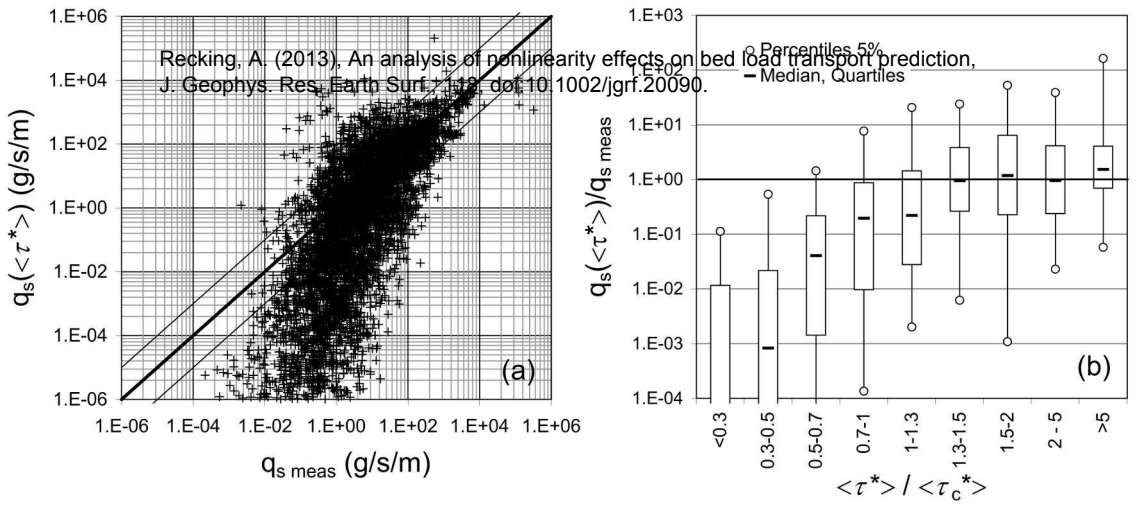
Recking, A. (2013), An analysis of nonlinearity effects on bed load transport prediction,
J. Geophys. Res. Earth Surf., 118, doi:10.1002/jgrf.20090.
(a)
$q_s(<\tau^*>)$ (g/s/m)
$q_{s\,meas}$ (g/s/m)
1.E-06
1.E-04
1.E-02
1.E+00
1.E+02
1.E+04
1.E+06
(b)
Percentiles 5%
Median, Quartiles
$q_s(<\tau^*>)/q_{s\,meas}$
1.E+03
1.E+02
1.E+01
1.E+00
1.E-01
1.E-02
1.E-03
1.E-04
<0.3
0.3-0.5
0.5-0.7
0.7-1
1-1.3
1.3-1.5
1.5-2
2 - 5
>5
$<\tau^*> / <\tau_c^*>$

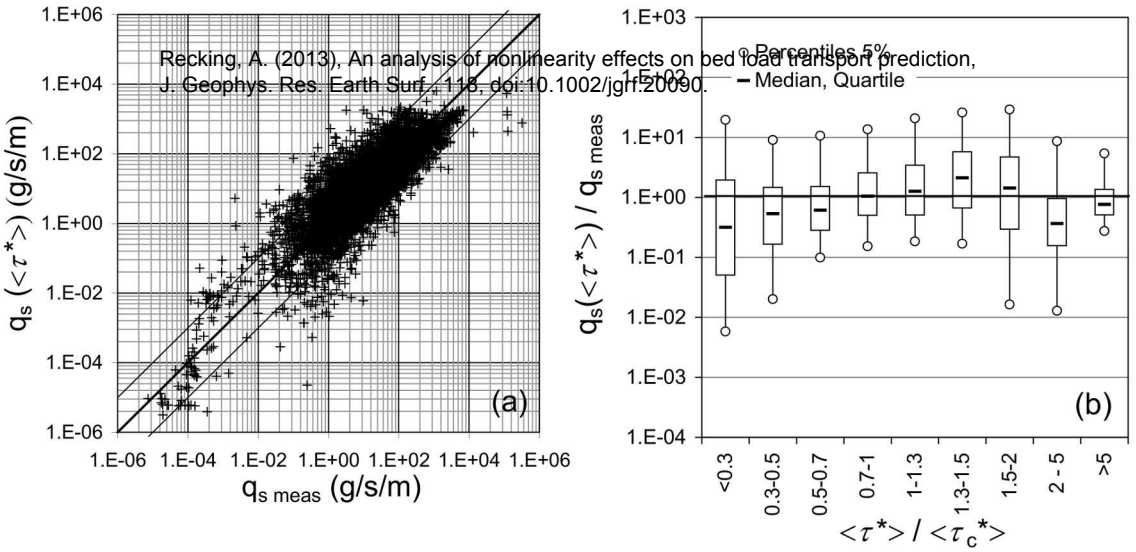
Recking, A. (2013), An analysis of nonlinearity effects on bed load transport prediction,
J. Geophys. Res. Earth Surf., 118, doi:10.1002/jgrf.20090.
1.E+06
1.E+04
1.E+02
1.E+00
1.E-02
1.E-04
1.E-06
q_s ($<\tau^*>$) (g/s/m)
1.E-06 1.E-04 1.E-02 1.E+00 1.E+02 1.E+04 1.E+06
$q_{s\ meas}$ (g/s/m)
(a)
1.E+03
1.E+02
1.E+01
1.E+00
1.E-01
1.E-02
1.E-03
1.E-04
$q_s(<\tau^*>)$ / $q_{s\ meas}$
Percentiles 5%
Median, Quartile
(b)
<0.3
0.3-0.5
0.5-0.7
0.7-1
1-1.3
1.3-1.5
1.5-2
2 - 5
>5
$<\tau^*>$ / $<\tau_c^*>$

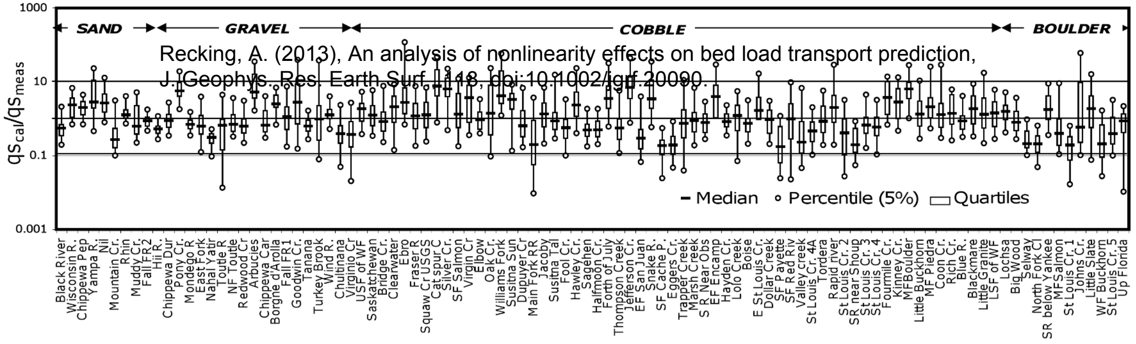

Recking, A. (2013), An analysis of nonlinearity effects on bed load transport prediction, J. Geophys. Res. Earth Surf., 118, doi:10.1002/jgrf.20090.

2013), An analysis of nonlinearity effects on bed load transpo
Res. Earth Surf., 118, doi:10.1002/jgrf.20090.

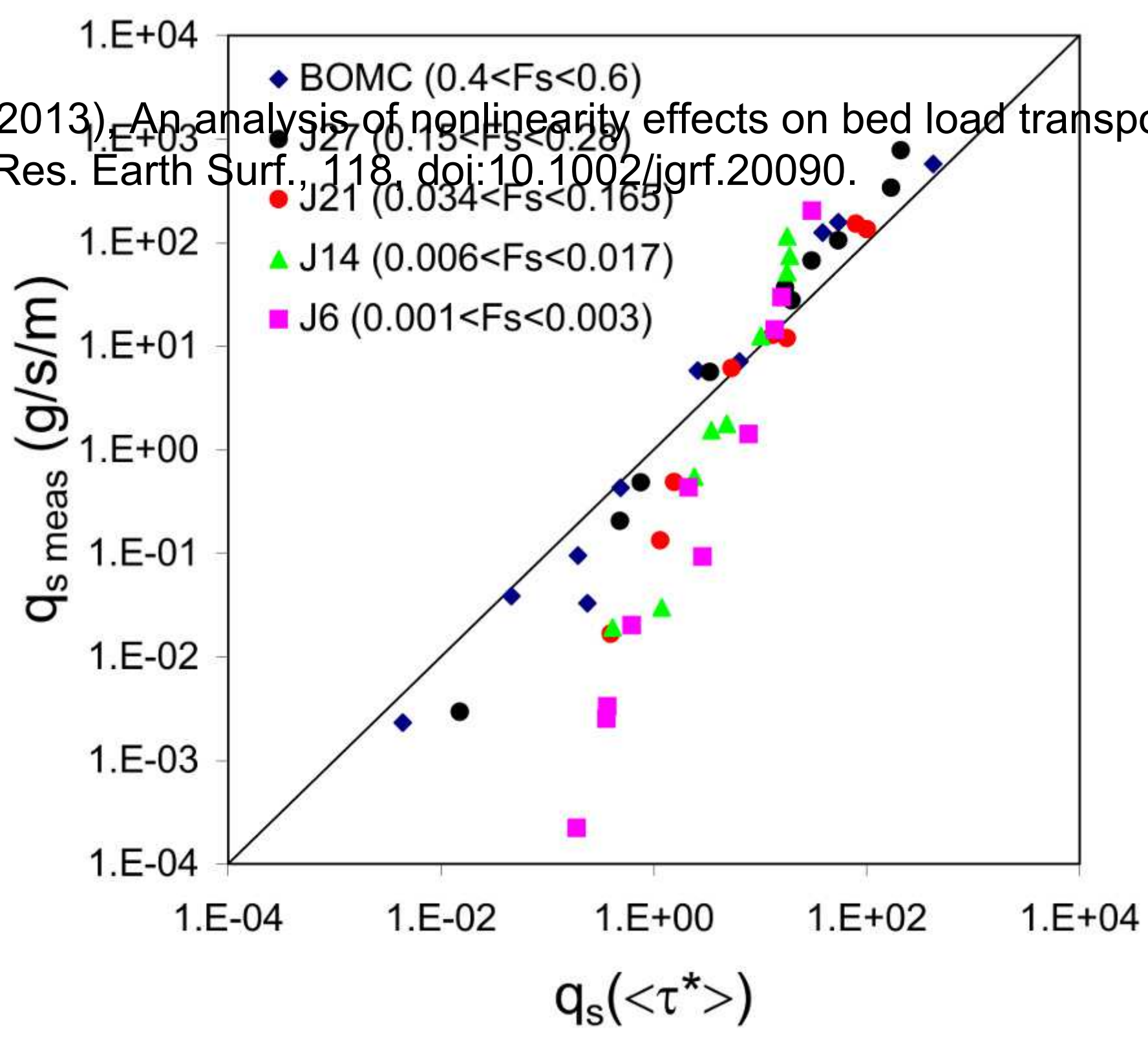

2013), An analysis of nonlinearity effects on bed load transpo
Res. Earth Surf., 118, doi:10.1002/jgrf.20090.

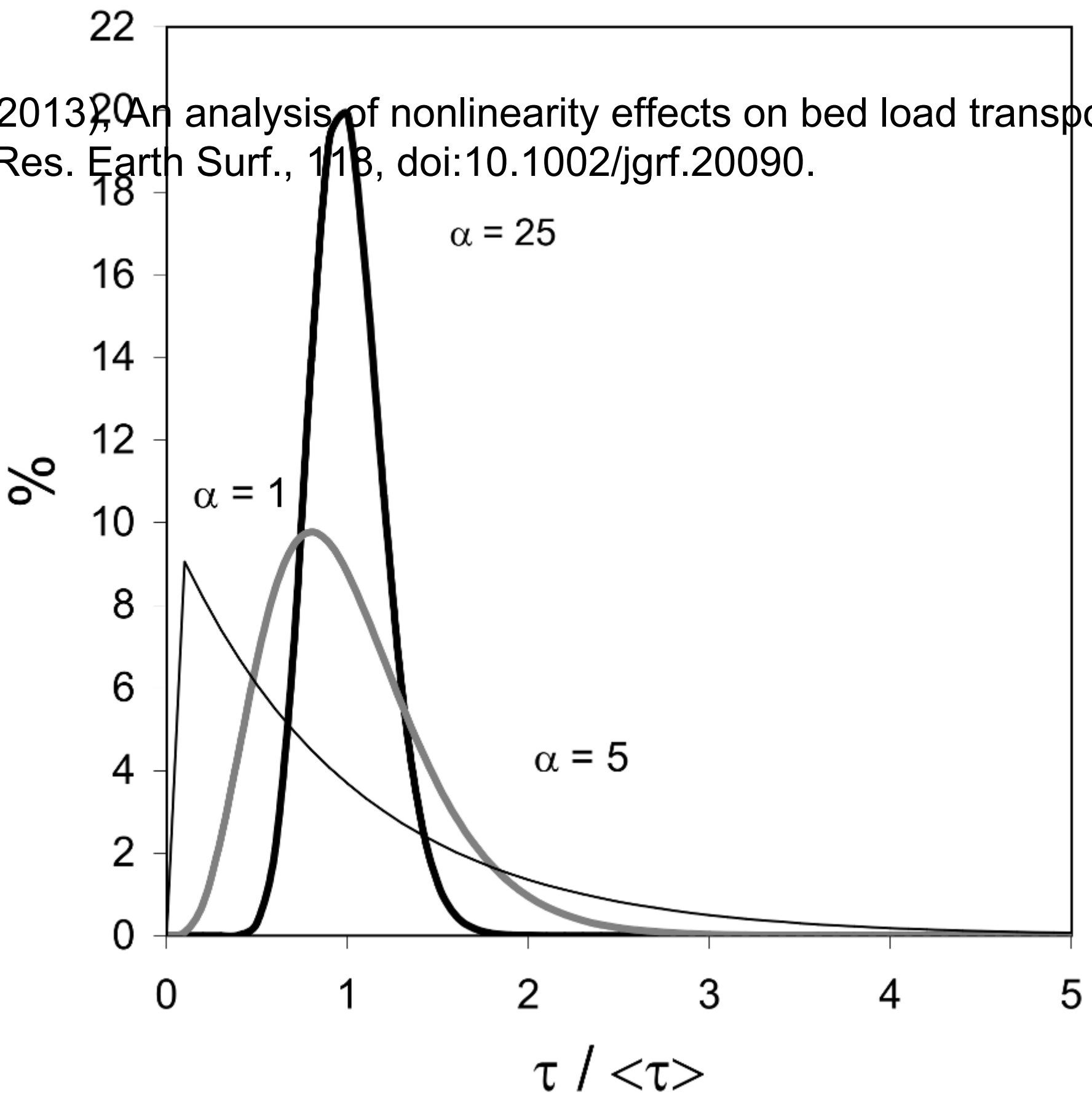

Recking, A. (2013), An analysis of nonlinearity effects on bed load transport prediction, J. Geophys. Res. Earth Surf., 118, doi:10.1002/jgrf.20090.

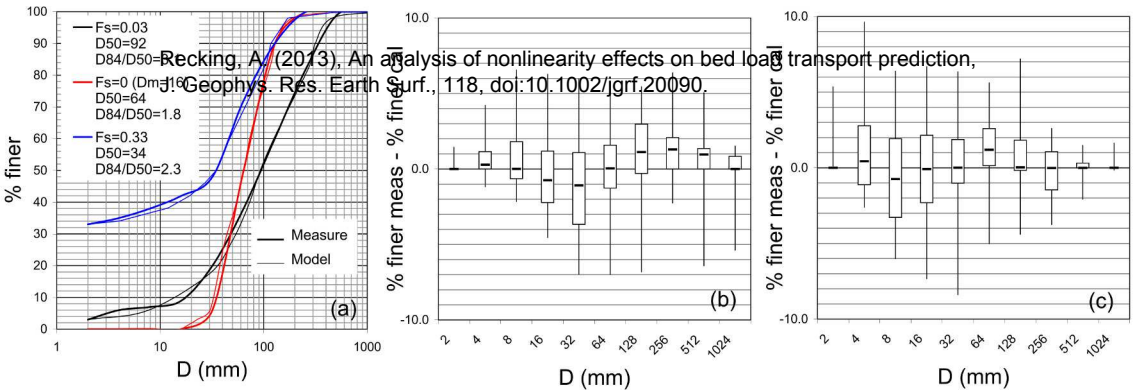

2013), An analysis of nonlinearity effects on bed load transpo
Res. Earth Surf., 118, doi:10.1002/jgrf.20090.

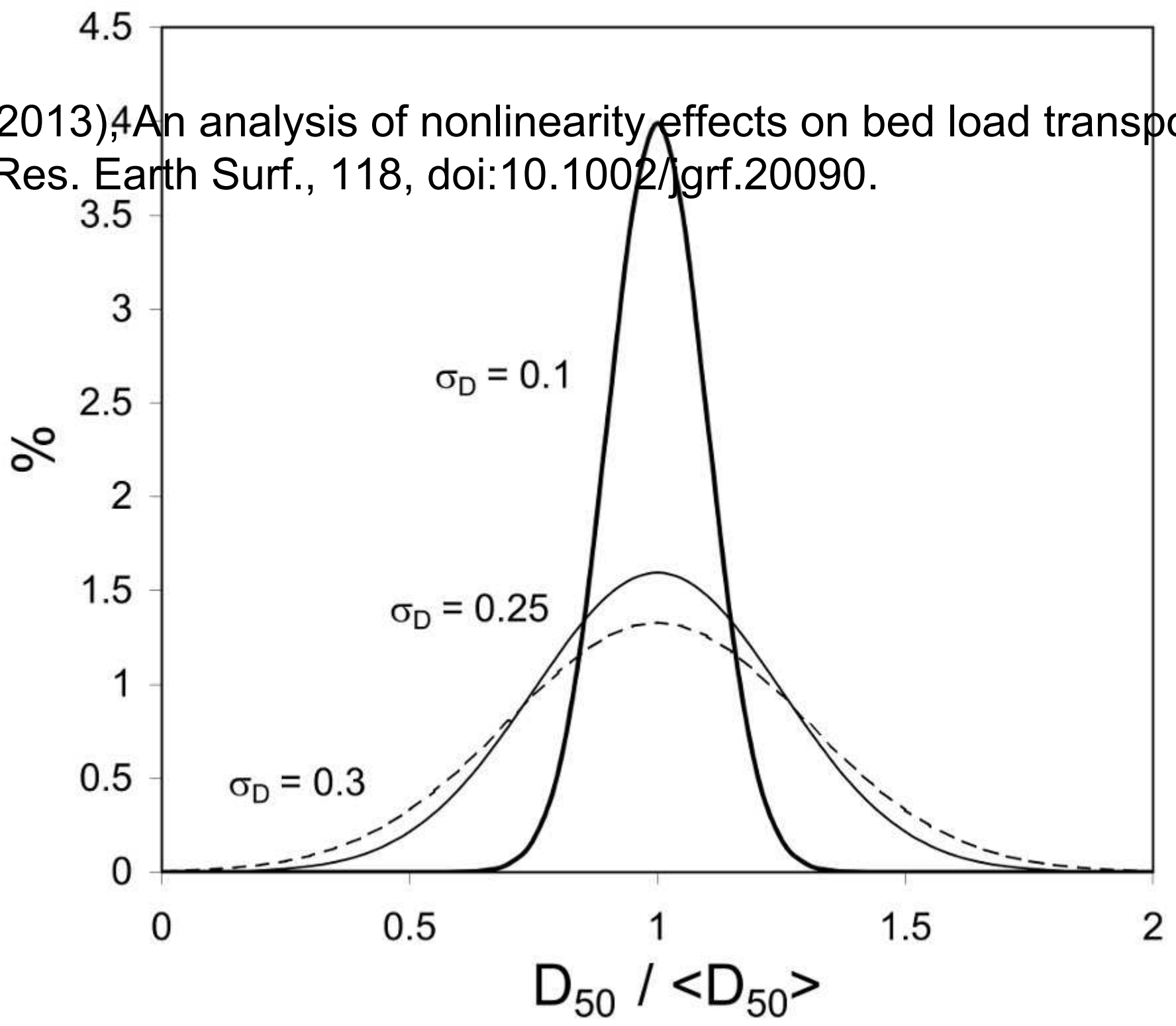

2013), An analysis of nonlinearity effects on bed load transpo
Res. Earth Surf., 118, doi:10.1002/jgrf.20090.

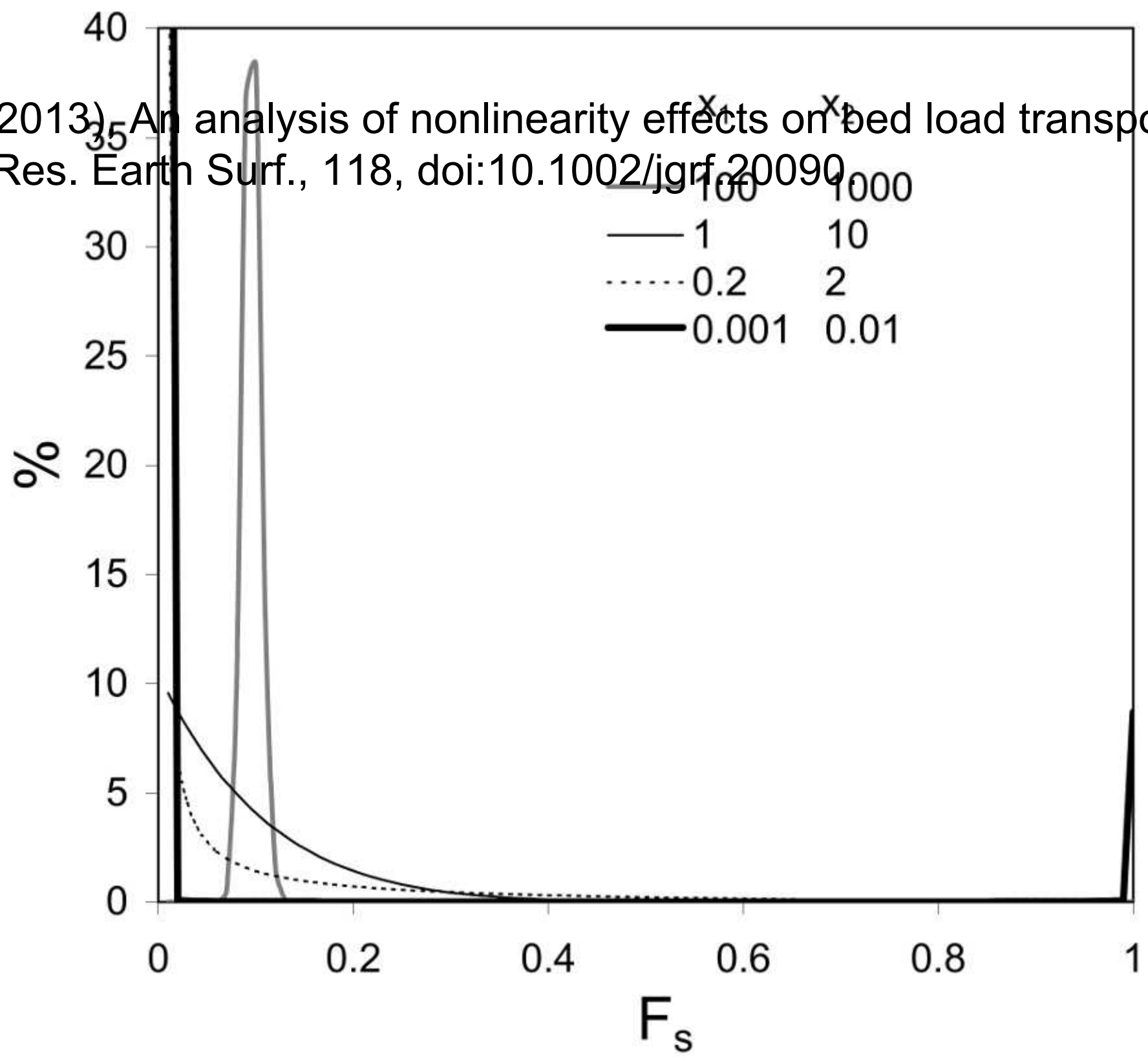

2013), An analysis of nonlinearity effects on bed load transpo
Res. Earth Surf., 118, doi: 10.1002/jgrf.20090.

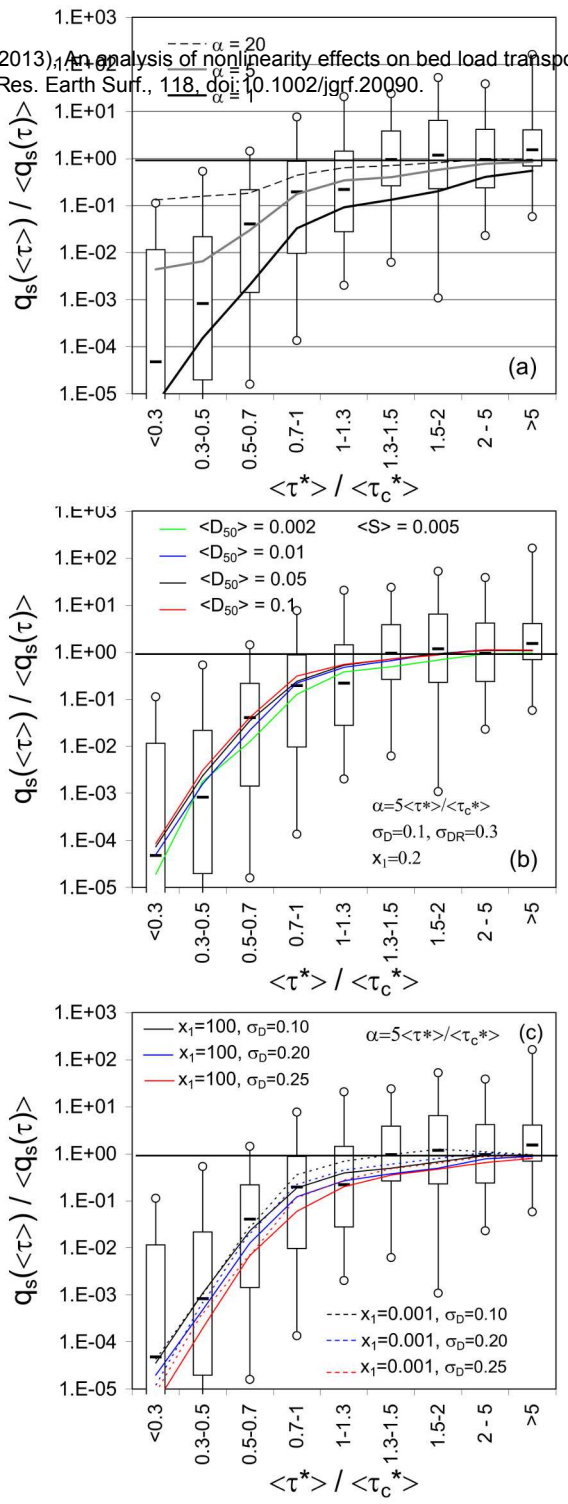

2013), An analysis of nonlinearity effects on bed load transpo
Res. Earth Surf., 118, doi:10.1002/jgrf.20090.

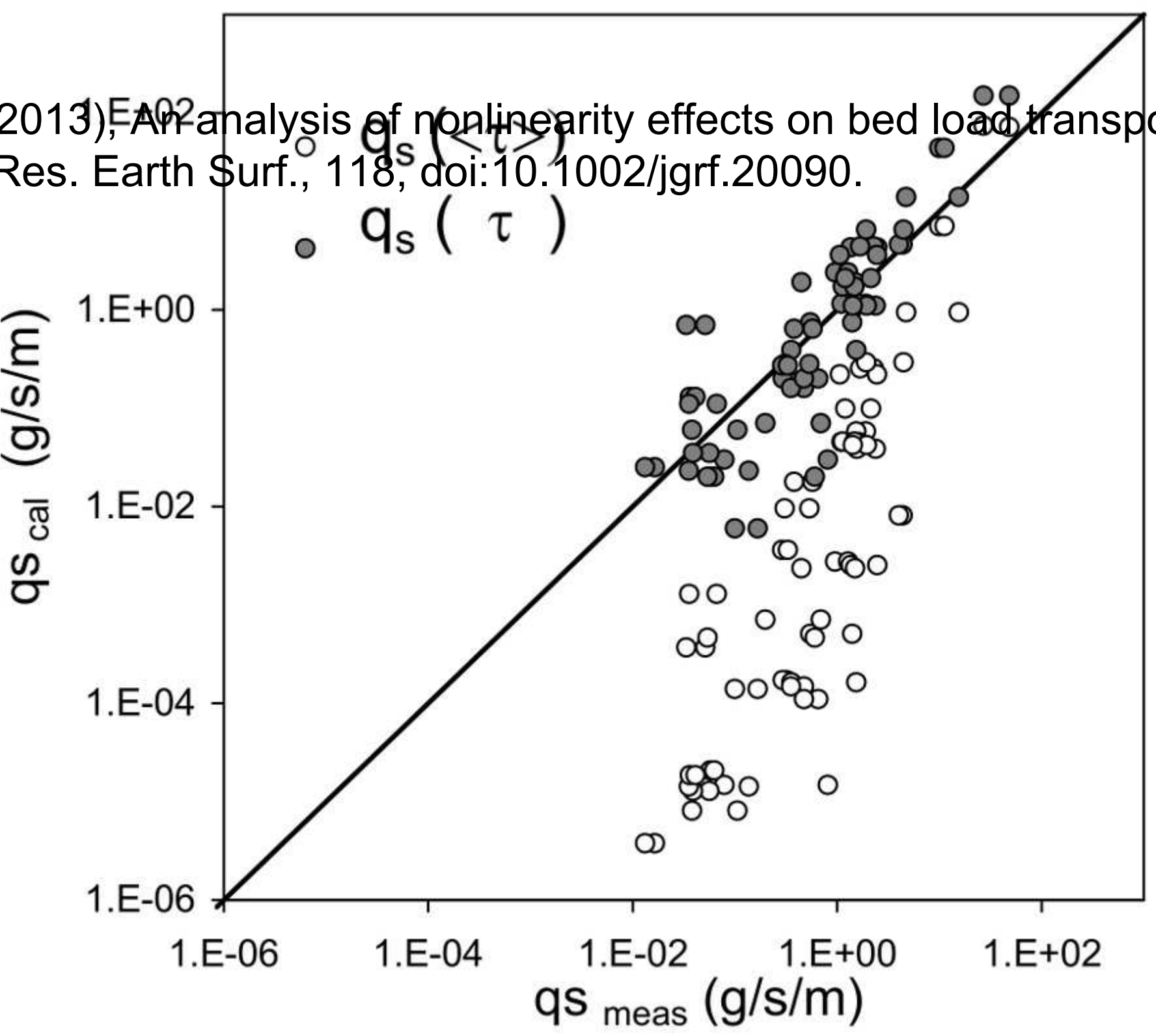

2013), An analysis of nonlinearity effects on bed load transpo
Res. Earth Surf., 118, doi:10.1002/jgrf.20090.